This paper appears in Control Engineering Practice, 2012.
http://dx.doi.org/10.1016/j.conengprac.2012.10.008

Nonlinear Disturbance Observer Design For Robotic Manipulators

A. Mohammadi[a,*], M. Tavakoli[b,**], H. J. Marquez[b], F. Hashemzadeh[b],

[a] *Edward S. Rogers Sr. Department of Electrical & Computer Engineering, University of Toronto, Toronto, Ontario, Canada M5S 3G4*
[b] *Department of Electrical & Computer Engineering, University of Alberta, Edmonton, Alberta, Canada T6G 2V4*

Abstract

Robotic manipulators are highly nonlinear and coupled systems that are subject to different types of disturbances such as joint frictions, unknown payloads, varying contact points, and unmodeled dynamics. These disturbances, when unaccounted for, adversely affect the performance of the manipulator. Employing a disturbance observer is a common method to reject such disturbances. In addition to disturbance rejection, disturbance observers can be used in force control applications. Recently, research has been done regarding the design of nonlinear disturbance observers (NLDOs) for robotic manipulators. In spite of good results in terms of disturbance tracking, the previously designed nonlinear disturbance observers can merely be used for planar serial manipulators with revolute joints (Chen, W.H., Ballance, D.J., Gawthorp, P.J., O'Reilly, J., 2000. A nonlinear disturbance observer for robotic manipulators. IEEE Trans. Ind. Electron. 47, 932–938), (Nikoobin, A., Haghighi, R., 2009. Lyapunov-based nonlinear disturbance observer for serial n-link manipulators. J. Intell. Robot. Syst. 55, 135–153). In this paper, a general systematic approach is proposed to solve the disturbance observer design problem for robotic manipulators without restrictions on the number of degrees-of-freedom (DOFs), the types of joints, or the manipulator configuration. Moreover, this design method does not need the exact dynamic model of the serial robotic manipulator. This method also

[*] Corresponding author, Tel.: +1 (647)978-0140
[**] Principal corresponding author, Tel.: +1 (780)492-8935, fax: +1 (780)492-1811
Email addresses: alireza.mohammadi@mail.utoronto.ca (A. Mohammadi), mahdi.tavakoli@ualberta.ca (M. Tavakoli), hmarquez@ualberta.ca (H. J. Marquez), farzad.hashemzadeh@ualberta.ca (F. Hashemzadeh)

unifies the previously proposed linear and nonlinear disturbance observers in a general framework. Simulations are presented for a 4-DOF SCARA manipulator to show the effectiveness of the proposed disturbance observer design method. Experimental results using a PHANToM Omni haptic device further illustrate the effectiveness of the design method.

Keywords: Nonlinear disturbance observer (NLDO), robotic manipulator, disturbance rejection, position control, force control, linear matrix inequality (LMI).

---

1. Introduction

Robotic manipulators are subject to different types of disturbances that adversely affect their performance such as positioning accuracy and repeatability; it is, therefore, imperative to employ some form of disturbance suppression or attenuation in order to achieve the desired performance. Adaptive control (Danesh et al., 2005), (Kim et al., 2008), active Kalman filtering (Cortesao, 2007), (Ji and Sul, 1995), H_∞ control (Khelfi and Abdessameud, 2007), (Sato and Tsuruta, 2006), predictive control (Cassemiro et al., 2005), (Bauchspiess et al., 2001) and sliding mode control (Corradini et al., 2012), (Pi and Wang, 2011), (Parlakci et al., 2004), are among the disturbance rejection techniques proposed in the literature for robotic applications.

An alternative to these techniques that has emerged in recent years is the use of the so-called "disturbance observers"(Ohnishi et al., 1996). Figure 1 shows the block diagram of a typical disturbance observer that is used in a robotic application. Roughly speaking, the idea behind the disturbance observer is to lump all the internal and external unknown torques/forces acting on the manipulator into a single disturbance term and then estimate this unknown term using the disturbance observer.

The output of the disturbance observer can be used in feedforward compensation of disturbances. Because of the feedforward nature of this compensation, disturbance observers can provide fast, excellent tracking performance and smooth control actions without the use of large feedback gains (Liu and Peng, 1997). For instance, a disturbance observer might be used in independent joint control where joint couplings, load variations and dynamic uncertainties are collectively treated as the lumped disturbance term (Zhongyi et al., 2008), (Park and Lee, 2007), (Choi and Kwak, 2003), (Eom et al., 1997), (Komada et al., 1996), (Hu and Muller, 1996). Efficient suppression of these disturbances decouples the dynamics of the joints and allows simple controllers to be designed for each DOF. Another

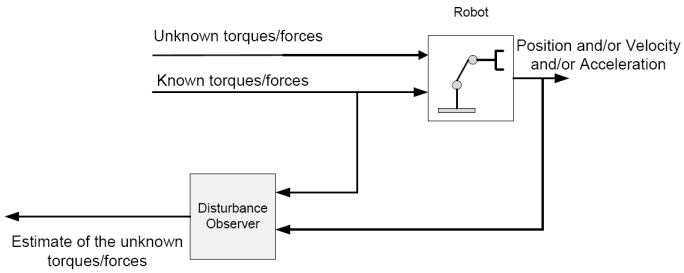

Figure 1: Block diagram of a typical disturbance observer in a robotic application.

application of disturbance observers is in improving manipulator tracking performance through friction estimation and compensation (Bona and Indri, 2005), (Sawut et al., 2001). In (Mohammadi et al., 2011a), the authors proposed a nonlinear disturbance observer- based control law that guaranteed asymptotic trajectory and disturbance tracking in the presence of slow-varying disturbances.

One important aspect of disturbance observer-based friction compensation schemes is in that they are not based on any particular friction models (Bona and Indri, 2005). Disturbance observers have recently been used in time-delayed bilateral teleoperation in order to improve the transparency of telerobotic systems (Natori et al., 2010), (Natori et al., 2007) and (Natori et al., 2006). In time-delayed teleoperation, the delayed position/force signals are received from the communication channel in the master and the slave sides. The time-delayed position/force signals are then added to the output of the disturbance observer in order to provide the master and the slave robots with estimation of the undelayed versions of the position/force signals and thus improve the teleoperation system transparency (Natori et al., 2010). In (Mohammadi et al., 2011b), the authors implemented a pair of nonlinear disturbance observers in a 4-channel bilateral teleoperation architecture to achieve full transparency in the absence of communication time delays in both free and constrained motions. In that work, however, the availability of joint acceleration measurements, which is necessary for achieving full transparency, simplified design of disturbance observers.

Besides disturbance rejection, disturbance observers have found applications in other robotics contexts. In many robotics applications, the robot end-effector comes in contact with a compliant surface and a force control scheme is needed to guarantee good system performance. Therefore, a force sensor is needed to measure these contact forces. Disturbance observers

can be employed in these applications when there is no sensor available for measuring torques and forces. For instance, disturbance observers have been employed successfully in sensorless force control (Shimada et al., 2010), (Katsura et al., 2003), (Eom et al., 1998), (Lee et al., 1993). Another potential application of disturbance observers can be in micro/nano manipulation tasks, e.g., microinjection to introduce foreign materials into biological cells (Tan et al., 2008), where there is a lack of small enough force sensors with good precision and signal to noise ratio (Rakotondrabe et al., 2010).

Recently, a new system has been developed to teach motion to robots in order to improve their dexterity (Katsura et al., 2010). The so-called *shadow robot system* consists of two identical robots. The robots are controlled by bilateral acceleration control schemes based on a disturbance observer. One robot is guided by a human operator in teaching motion mode and the other robot is unconstrained and imitates the motion of the constrained robot with the same position, velocity and acceleration. It is desired that the human operator's pure force is extracted from the constrained robot. In order to find the operator's force, a disturbance observer is employed to estimate the disturbance forces such as friction and gravity in the unconstrained robot. The disturbance forces acting on the constrained and the unconstrained robots are the same. The human operator's force is then estimated by subtracting the disturbance forces acting on the unconstrained robot from the total force in the constrained robot. As a result, the shadow robot system observes the human force in the presence of gravity and friction without a need for force sensors. Lastly, industrial robots employ fault detection systems in order to determine if a fault, such as a collision or an abrupt increase in reaction forces, has occurred in the system. Disturbance observers have been used for fault detection in a number of robotic applications (Sneider and Frank, 1996), (Chan, 1995), (Ohishi and Ohde, 1994). Table 1 summarizes the most important applications of disturbance observers in robotics.

A considerable part of the existing literature on disturbance observer design for robotic applications uses linearized models or linear system techniques (Komada et al., 2000), (Liu and Peng, 2000), (Bickel and Tomizuka, 1995), (Kim and Chung, 2003). In order to overcome the linear disturbance observer limitations for the highly nonlinear and coupled dynamics of robotic manipulators, Chen et al. proposed a general nonlinear disturbance observer structure for nonlinear robotic manipulators (Chen et al., 2000). Using Chen et al. NDOB, the observer design problem reduces to finding an observer gain matrix such that disturbance tracking is achieved. However, Chen et al. could find such a gain matrix for a 2-link planar manipulator with revolute joints. Later, Nikoobin et al. generalized Chen's solution to

Disturbance rejection	Independent joint control	(Zhongyi et al., 2008), (Park and Lee, 2007), (Choi and Kwak, 2003), (Eom et al., 1997), (Komada et al., 1996), (Hu and Muller, 1996)
	Friction estimation and compensation	(Bona and Indri, 2005), (Sawut et al., 2001) (Mohammadi et al., 2011a)
	Time-delayed and transparent teleoperation control	(Mohammadi et al., 2011b), (Natori et al., 2010), (Natori et al., 2007), (Natori et al., 2006)
Force/torque estimation	Sensorless force control	(Shimada et al., 2010), (Katsura et al., 2003), (Eom et al., 1998), (Lee et al., 1993)
	Shadow robot system	(Katsura et al., 2010)
	Fault detection	(Sneider and Frank, 1996), (Chan, 1995), (Ohishi and Ohde, 1994)

Table 1: Disturbance observer applications in robotics

n-link planar manipulators with revolute joints by exploiting the explicit relation for this particular class of robots (Nikoobin and Haghighi, 2009). In addition to limitations on manipulator configuration, their design could not guarantee exponential disturbance tracking and merely proved asymptotic disturbance tracking. Both (Chen et al., 2000) and (Nikoobin and Haghighi, 2009) used explicit formulae for the inertia matrices of a particular class of manipulators to solve the disturbance observer design problem. Although these disturbance observers show promising results in disturbance estimation, their design is limited to planar, serial manipulators with revolute joints. Industrial robots including 6-DOF articulated robotic arms such as EPSON C3 and PUMA 560 are, however, non-planar. Moreover, some of the industrial arms such as SCARA manipulators have prismatic joints in addition to revolute joints. This serves as the motivation to look for a general design method.

In this paper, the objective is to solve the NDOB design problem, proposed by Chen et al., for the class of all serial manipulators. The design method removes the existing restrictions on the number of DOFs, joint types, or manipulator configuration by invoking general dynamic properties common in all serial manipulators. Moreover, the design method does not require knowing the full dynamics of the robot. A novel inequality will be derived that can be used to design nonlinear disturbance observers for all serial robotic manipulators. The disturbance observer design problem will be formulated as a linear matrix inequality (LMI), which can be readily solved using LMI software packages such as the MATLAB LMI Control Toolbox (Gahinet et al., 1995). In addition to the LMI formulation, an analytical solution to the design problem will be presented.

The organization of this paper is as follows. Section 2 introduces the

nonlinear disturbance observer structure and its modified version, which does not need joint acceleration measurements. Section 3 solves the design problem for nonlinear disturbance observers and gives sufficient conditions for global asymptotic and exponential disturbance tracking for the case of slow-varying disturbances, and global uniform ultimate boundedness of the disturbance tracking error for the case of fast-varying disturbances. The observer design problem will also be formulated as a linear matrix inequality. In Section 4, important issues that should be considered in the design of disturbance observers are addressed. This Section concludes with an analytical solution to the observer design problem. Section 5 shows the effectiveness of the proposed design method by performing simulations on a SCARA manipulator, a 4-DOF industrial arm, where the designed nonlinear disturbance observer is used to estimate and compensate for the joint friction and external end-effector payloads. Experiments are carried out using a PHANToM Omni haptic device in Section 6 to show the effectiveness of the designed observer in terms of improving position tracking via a computed-torque control scheme. Both in the simulations and the experiments, we have compared the performance of the proposed approach with some other well-known techniques available in the literature. Lastly, Section 7 includes the concluding remarks.

2. Nonlinear disturbance observer structure

In this section, the dynamic model of serial robotic manipulators and their properties are introduced. Next, a basic disturbance observer that needs acceleration measurements will be introduced. Then, the disturbance observer will be modified in a way that acceleration measurement is no longer needed.

2.1. Dynamic model of serial robotic manipulators

The following equation gives the dynamics of an n-DOF rigid serial manipulator (Spong et al., 2005):

$$\mathbf{M}(\mathbf{q})\ddot{\mathbf{q}} + \mathbf{N}(\mathbf{q}, \dot{\mathbf{q}}) + \mathbf{F}(\dot{\mathbf{q}}) = \boldsymbol{\tau} + \boldsymbol{\tau}_{ext}, \tag{1}$$

where,

$$\mathbf{N}(\mathbf{q}, \dot{\mathbf{q}}) = \mathbf{C}(\mathbf{q}, \dot{\mathbf{q}})\dot{\mathbf{q}} + \mathbf{G}(\mathbf{q}), \tag{2}$$

and, $\mathbf{q} \in R^{n\times 1}$ is the vector of joint positions, $\mathbf{M}(\mathbf{q}) \in R^{n\times n}$ is the inertia matrix, $\mathbf{F}(\dot{\mathbf{q}})$ is the vector of joint friction torques, $\mathbf{C}(\mathbf{q}, \dot{\mathbf{q}})\dot{\mathbf{q}} \in R^{n\times 1}$ is the

vector of Coriolis and centrifugal forces, $\mathbf{G}(\mathbf{q}) \in R^{n\times 1}$ is the gravity vector, $\boldsymbol{\tau} \in R^{n\times 1}$ is the vector of the control torques applied to the joints, and $\boldsymbol{\tau}_{ext} \in R^{n\times 1}$ is the vector of the external disturbances exerted to the joints.

It is assumed that the manipulator velocity vector lies in a bounded set, i.e.,

$$\dot{\mathbf{q}} \in D_{\dot{\mathbf{q}}} = \{\dot{\mathbf{q}} \in R^n : ||\dot{\mathbf{q}}|| \leq ||\dot{\mathbf{q}}||_{max}\}. \tag{3}$$

The set in which the robot joint variables vary (i.e., the robot workspace) is denoted by $D_{\mathbf{q}}$. It is assumed that $D_{\mathbf{q}}$ is a bounded set. This assumption ensures that the manipulator's prismatic joints do not extend to infinity, which is true in all physical manipulators.

Serial robotic manipulators have several inherent dynamic properties, which will be used when designing the disturbance observer later in this paper. These properties are listed below.

Property 1. The inertia matrix $\mathbf{M}(\mathbf{q})$ is symmetric and positive definite and its norm[1] is bounded (Spong et al., 2005):

$$\mathbf{M}(\mathbf{q}) = \mathbf{M}^T(\mathbf{q}) > \mathbf{0}, \tag{4}$$

$$\forall \mathbf{q} \in D_{\mathbf{q}},\ \nu_1(\mathbf{q}) \leq ||\mathbf{M}(\mathbf{q})|| \leq \nu_2(\mathbf{q}), \tag{5}$$

where $\nu_1(\mathbf{q})$ and $\nu_2(\mathbf{q})$ are scalar functions of the joint position vector $\mathbf{q}$. Defining $\nu_1 = \inf_{\mathbf{q}\in D_{\mathbf{q}}} \{\sigma_1(\mathbf{q})\}$ and $\nu_2 = \sup_{\mathbf{q}\in D_{\mathbf{q}}} \{\sigma_2(\mathbf{q})\}$, it can be seen that

$$\nu_1 \leq ||\mathbf{M}(\mathbf{q})|| \leq \nu_2, \forall \mathbf{q} \in D_{\mathbf{q}}. \tag{6}$$

Property 2. The matrix $\dot{\mathbf{M}}(\mathbf{q}) - 2\mathbf{C}(\mathbf{q}, \dot{\mathbf{q}})$ is skew-symmetric (Spong et al., 2005); namely,

[1]Throughout the paper, unless otherwise stated, by a vector norm, the vector 2-norm is meant and by a matrix norm, the induced matrix 2-norm is meant:

$$\mathbf{x} \in R^n \Rightarrow ||\mathbf{x}|| = \sqrt{\mathbf{x}^T\mathbf{x}},$$
$$\mathbf{X} \in R^{n\times n} \Rightarrow ||\mathbf{X}|| = \sqrt{\lambda_{max}(\mathbf{X}^T\mathbf{X})},$$

where $\lambda_{max}(.)$ denotes the maximum eigenvalue of a square matrix.

$$[\dot{\mathbf{M}}(\mathbf{q}) - 2\mathbf{C}(\mathbf{q},\dot{\mathbf{q}})]^T = -[\dot{\mathbf{M}}(\mathbf{q}) - 2\mathbf{C}(\mathbf{q},\dot{\mathbf{q}})]$$
$$\Rightarrow \dot{\mathbf{M}}(\mathbf{q}) = \mathbf{C}(\mathbf{q},\dot{\mathbf{q}}) + \mathbf{C}^T(\mathbf{q},\dot{\mathbf{q}}). \tag{7}$$

Property 3. The Coriolis/centrifugal matrix $\mathbf{C}(\mathbf{q},\dot{\mathbf{q}})$ has an upper bounded induced 2-norm (Mulero-Martinez, 2007):

$$\forall \mathbf{q} \in D_{\mathbf{q}}, \;\; ||\mathbf{C}(\mathbf{q},\dot{\mathbf{q}})|| \leq C_b(\mathbf{q})||\dot{\mathbf{q}}||^2, \tag{8}$$

where $C_b(\mathbf{q})$ is a scalar function of the joint position vector $\mathbf{q}$.
Defining $\delta = \sup_{\mathbf{q}\in D_{\mathbf{q}}} \{C_b(\mathbf{q})\}$ and using (3), from (8) it is observed that

$$||\mathbf{C}(\mathbf{q},\dot{\mathbf{q}})|| \leq \delta||\dot{\mathbf{q}}||^2_{max}. \tag{9}$$

Also note that (7) and (9) imply

$$||\dot{\mathbf{M}}(\mathbf{q})|| \leq 2\delta||\dot{\mathbf{q}}||^2_{max}. \tag{10}$$

Remark. If all joints of the manipulator are revolute, the scalar function $C_b(\mathbf{q})$ in (8) will become a constant and $\mathbf{C}(\mathbf{q},\dot{\mathbf{q}})$ is said to be uniformly bounded. In this case, an upper bound of $C_b(\mathbf{q})$ is given as (Mulero-Martinez, 2007):

$$\delta = \frac{3}{2} \sup_{\mathbf{q}\in D_{\mathbf{q}}} \{\sum_{i=1}^{n} ||\frac{\partial \mathbf{M}(\mathbf{q})}{\partial q_i}||\}. \tag{11}$$

The above equation can be used efficiently to determine an upper bound of $||\dot{\mathbf{M}}(\mathbf{q})||$ for articulated robots.

$\diamondsuit$

Now, assume that $\hat{\mathbf{M}}(\mathbf{q})$ and $\hat{\mathbf{N}}(\mathbf{q},\dot{\mathbf{q}})$ are the estimates of the actual $\mathbf{M}(\mathbf{q})$ and $\mathbf{N}(\mathbf{q},\dot{\mathbf{q}})$, and that $\Delta\mathbf{M}$ and $\Delta\mathbf{N}$ are the corresponding additive uncertainties present in the model of the robot:

$$\mathbf{M}(\mathbf{q}) = \hat{\mathbf{M}}(\mathbf{q}) + \Delta\mathbf{M}, \tag{12}$$
$$\mathbf{N}(\mathbf{q},\dot{\mathbf{q}}) = \hat{\mathbf{N}}(\mathbf{q},\dot{\mathbf{q}}) + \Delta\mathbf{N}. \tag{13}$$

The lumped disturbance vector $\boldsymbol{\tau}_d$ is defined as

$$\boldsymbol{\tau}_d = \boldsymbol{\tau}_{ext} - \Delta\mathbf{M}\ddot{\mathbf{q}} - \Delta\mathbf{N} - \mathbf{F}(\dot{\mathbf{q}}). \tag{14}$$

By this definition, the effect of all dynamic uncertainties, joint frictions and external disturbances is lumped into a single disturbance vector $\boldsymbol{\tau}_d$. From (1), it is seen that

$$\hat{\mathbf{M}}(\mathbf{q})\ddot{\mathbf{q}} + \hat{\mathbf{N}}(\mathbf{q}, \dot{\mathbf{q}}) = \boldsymbol{\tau} + \boldsymbol{\tau}_d. \tag{15}$$

Inspired by the inherent dynamic characteristics of serial robotic manipulators, the inertia matrix estimate $\hat{\mathbf{M}}(\mathbf{q})$ is chosen to satisfy the following properties:

- $\hat{\mathbf{M}}(\mathbf{q})$ is symmetric, positive definite and uniformly bounded. That is, the following relations hold:

$$\hat{\mathbf{M}}(\mathbf{q}) = \hat{\mathbf{M}}^T(\mathbf{q}) > \mathbf{0}, \tag{16}$$

$$\forall \mathbf{q} \in D_{\mathbf{q}},\ \sigma_1 \mathbf{I} \leq \hat{\mathbf{M}}(\mathbf{q}) \leq \sigma_2 \mathbf{I}, \tag{17}$$

  where σ_1 and σ_2 are two positive real constants. Also, $\mathbf{I}$ is the identity matrix.

- The 2-norm of $\dot{\hat{\mathbf{M}}}(\mathbf{q})$ is bounded. That is to say

$$\forall \mathbf{q} \in D_{\mathbf{q}},\ ||\dot{\hat{\mathbf{M}}}(\mathbf{q})|| \leq \zeta, \tag{18}$$

  where ζ is a positive real constant.

Remark. $\hat{\mathbf{M}}(\mathbf{q})$ can be any arbitrary matrix satisfying (16), (17) and (18). For instance, $\hat{\mathbf{M}}(\mathbf{q})$, can be a constant, positive definite and symmetric matrix. As another example, the estimated Denavit-Hartenberg (D-H) parameters of a robot may be used to find the estimate of its inertia matrix.

$\diamondsuit$

2.2. Basic disturbance observer structure

Assuming joint acceleration measurements are available, the following nonlinear disturbance observer has been proposed for the robot (15) by (Chen et al., 2000):

$$\dot{\hat{\boldsymbol{\tau}}}_d = -\mathbf{L}\hat{\boldsymbol{\tau}}_d + \mathbf{L}\{\hat{\mathbf{M}}(\mathbf{q})\ddot{\mathbf{q}} + \hat{\mathbf{N}}(\mathbf{q}, \dot{\mathbf{q}}) - \boldsymbol{\tau}\}, \tag{19}$$

where $\mathbf{L}$ is the observer gain matrix. Defining $\Delta\boldsymbol{\tau}_d = \boldsymbol{\tau}_d - \hat{\boldsymbol{\tau}}_d$ as the disturbance tracking error and using (15), it is observed that

$$\dot{\hat{\boldsymbol{\tau}}}_d = \mathbf{L}\Delta\boldsymbol{\tau}_d, \tag{20}$$

or, equivalently,

$$\Delta\dot{\boldsymbol{\tau}}_d = \dot{\boldsymbol{\tau}}_d - \mathbf{L}\Delta\boldsymbol{\tau}_d. \tag{21}$$

2.3. Modified disturbance observer structure

The disadvantage of the disturbance observer (19) is the need for acceleration measurement. Accurate accelerometers are not available in many robotic systems. Unless robust differentiation techniques are employed (Levant, 1998), differentiating the noise-corrupted velocity signals is not a suitable option for deriving acceleration signals. It is possible to modify the disturbance observer, as in (Chen et al., 2000), in a way that no acceleration measurement is needed. For this purpose, the auxiliary variable $\mathbf{z}$ is defined as

$$\mathbf{z} = \hat{\boldsymbol{\tau}}_d - \mathbf{p}(\mathbf{q}, \dot{\mathbf{q}}), \tag{22}$$

where the vector $\mathbf{p}(\mathbf{q}, \dot{\mathbf{q}})$ can be determined from the modified observer gain matrix $\mathbf{L}(\mathbf{q}, \dot{\mathbf{q}})$:

$$\frac{d}{dt}\mathbf{p}(\mathbf{q}, \dot{\mathbf{q}}) = \mathbf{L}(\mathbf{q}, \dot{\mathbf{q}})\hat{\mathbf{M}}(\mathbf{q})\ddot{\mathbf{q}}. \tag{23}$$

With (15), (19) and (23), taking the time derivative of (22) results in

$$\begin{aligned}
&\dot{\mathbf{z}} = \dot{\hat{\boldsymbol{\tau}}}_d - \dot{\mathbf{p}}(\mathbf{q}, \dot{\mathbf{q}}) = \dot{\hat{\boldsymbol{\tau}}}_d - \mathbf{L}(\mathbf{q}, \dot{\mathbf{q}})\hat{\mathbf{M}}(\mathbf{q})\ddot{\mathbf{q}} \Rightarrow \\
&\dot{\mathbf{z}} = -\mathbf{L}(\mathbf{q}, \dot{\mathbf{q}}) \underbrace{[\mathbf{z} + \mathbf{p}(\mathbf{q}, \dot{\mathbf{q}})]}_{\hat{\boldsymbol{\tau}}_d} + \\
&\mathbf{L}(\mathbf{q}, \dot{\mathbf{q}})\{\hat{\mathbf{M}}(\mathbf{q})\ddot{\mathbf{q}} + \hat{\mathbf{N}}(\mathbf{q}, \dot{\mathbf{q}}) - \boldsymbol{\tau} - \hat{\mathbf{M}}(\mathbf{q})\ddot{\mathbf{q}}\} \\
&\Rightarrow \dot{\mathbf{z}} = -\mathbf{L}(\mathbf{q}, \dot{\mathbf{q}})\mathbf{z} + \\
&\mathbf{L}(\mathbf{q}, \dot{\mathbf{q}})\{\hat{\mathbf{N}}(\mathbf{q}, \dot{\mathbf{q}}) - \boldsymbol{\tau} - \mathbf{p}(\mathbf{q}, \dot{\mathbf{q}})\}.
\end{aligned} \tag{24}$$

Therefore, the modified disturbance observer, which does not need acceleration measurement due to cancellation of the term $\mathbf{M}(\mathbf{q})\ddot{\mathbf{q}}$, takes the following form:

$$
\begin{aligned}
\dot{\mathbf{z}} &= -\mathbf{L}(\mathbf{q},\dot{\mathbf{q}})\mathbf{z} + \mathbf{L}(\mathbf{q},\dot{\mathbf{q}})\{\hat{\mathbf{N}}(\mathbf{q},\dot{\mathbf{q}}) - \boldsymbol{\tau} - \mathbf{p}(\mathbf{q},\dot{\mathbf{q}})\}, \\
\hat{\boldsymbol{\tau}}_d &= \mathbf{z} + \mathbf{p}(\mathbf{q},\dot{\mathbf{q}}), \\
\frac{d}{dt}\mathbf{p}(\mathbf{q},\dot{\mathbf{q}}) &= \mathbf{L}(\mathbf{q},\dot{\mathbf{q}})\hat{\mathbf{M}}(\mathbf{q})\ddot{\mathbf{q}}.
\end{aligned} \tag{25}
$$

From (25), the error dynamics becomes

$$
\begin{aligned}
&\Delta\dot{\boldsymbol{\tau}}_d = \dot{\boldsymbol{\tau}}_d - \dot{\hat{\boldsymbol{\tau}}}_d = \dot{\boldsymbol{\tau}}_d - \dot{\mathbf{z}} - \frac{d}{dt}\mathbf{p}(\mathbf{q},\dot{\mathbf{q}}) \\
&= \dot{\boldsymbol{\tau}}_d + \mathbf{L}(\mathbf{q},\dot{\mathbf{q}})\underbrace{[\hat{\boldsymbol{\tau}}_d - \mathbf{p}(\mathbf{q},\dot{\mathbf{q}})]}_{\mathbf{z}} - \mathbf{L}(\mathbf{q},\dot{\mathbf{q}})\{\underbrace{-\hat{\mathbf{M}}(\mathbf{q})\ddot{\mathbf{q}} + \boldsymbol{\tau}_d}_{\hat{\mathbf{N}}(\mathbf{q},\dot{\mathbf{q}})-\boldsymbol{\tau}} \\
&-\mathbf{p}(\mathbf{q},\dot{\mathbf{q}})\} - \mathbf{L}(\mathbf{q},\dot{\mathbf{q}})\hat{\mathbf{M}}(\mathbf{q})\ddot{\mathbf{q}} = \dot{\boldsymbol{\tau}}_d - \mathbf{L}(\mathbf{q},\dot{\mathbf{q}})(\boldsymbol{\tau}_d - \hat{\boldsymbol{\tau}}_d).
\end{aligned}
$$

Therefore, it is seen that

$$
\Delta\dot{\boldsymbol{\tau}}_d = \dot{\boldsymbol{\tau}}_d - \mathbf{L}(\mathbf{q},\dot{\mathbf{q}})\Delta\boldsymbol{\tau}_d. \tag{26}
$$

Note that the modified disturbance observer, which does not need acceleration measurement, has a similar error dynamics to the basic disturbance observer error dynamics (21).

In order to complete the disturbance observer design, the vector $\mathbf{p}(\mathbf{q},\dot{\mathbf{q}})$ and the matrix $\mathbf{L}(\mathbf{q},\dot{\mathbf{q}})$ should be determined. Finding such a gain matrix for the class of all serial manipulators is the main contribution of this papers that is the topic of the next section.

3. Nonlinear disturbance observer design

In this section, the main results of this paper will be presented, namely, a systematic method for the disturbance observer gain matrix design and the formulation of disturbance observer design problem in the form of a linear matrix inequality (LMI).

3.1. Disturbance observer design method

Given the disturbance observer (25), $\mathbf{p}(\mathbf{q},\dot{\mathbf{q}})$ and $\mathbf{L}(\mathbf{q},\dot{\mathbf{q}})$ should be determined to complete the disturbance observer design. The following disturbance observer gain matrix is proposed:

$$\mathbf{L}(\mathbf{q}) = \mathbf{X}^{-1}\hat{\mathbf{M}}^{-1}(\mathbf{q}), \tag{27}$$

where $\mathbf{X}$ is a constant invertible $n \times n$ matrix to be determined. Note that the estimate of the robot inertia matrix is chosen to be symmetric and positive definite and thus invertible. According to (23), it is seen that

$$\mathbf{p}(\dot{\mathbf{q}}) = \mathbf{X}^{-1}\dot{\mathbf{q}}. \tag{28}$$

In this way, nonlinear disturbance observer is given by (25) with the disturbance observer gain matrix $\mathbf{L}(\mathbf{q})$ in (27) and the disturbance observer auxiliary vector $\mathbf{p}(\dot{\mathbf{q}})$ in (28).

First, it will be assumed that the rate of change of the lumped disturbance is negligible in comparison with the disturbance estimation error dynamics, i.e., $\dot{\boldsymbol{\tau}}_d \approx \mathbf{0}$. This assumption is not overly restrictive and is commonly encountered in the robotics literature (see, for example, (Chen et al., 2000)). Next, the case when the robotic manipulator is experiencing fast-varying disturbances is considered. The following theorem states the sufficient conditions for asymptotic and exponential disturbance tracking when the robotic manipulator is subject to slow-varying disturbances.

Theorem 1. *Consider the serial robotic manipulator subject to disturbances described by* (15)*. The disturbance observer is given in* (25) *with the disturbance observer gain matrix* $\mathbf{L}(\mathbf{q})$ *defined in* (27) *and the disturbance observer auxiliary vector* $\mathbf{p}(\dot{\mathbf{q}})$ *defined in* (28)*. The disturbance tracking error* $\Delta\boldsymbol{\tau}_d$ *converges exponentially to zero for all* $\Delta\boldsymbol{\tau}_d(0) \in R^n$ *if the following conditions hold:*

1. *The matrix* $\mathbf{X}$ *is invertible,*
2. *There exists a positive definite and symmetric matrix* $\boldsymbol{\Gamma}$ *such that*[2]

$$\mathbf{X} + \mathbf{X}^T - \mathbf{X}^T\dot{\hat{\mathbf{M}}}(\mathbf{q})\mathbf{X} \geq \boldsymbol{\Gamma}. \tag{29}$$

3. $\dot{\boldsymbol{\tau}}_d \approx \mathbf{0}$*, i.e., the rate of change of the lumped disturbance acting on the manipulator is negligible in comparison with the estimation error dynamics* (26)*.*

[2]By $\mathbf{A} \geq \mathbf{B}$, where $\mathbf{A}$ and $\mathbf{B}$ are square matrices it is meant that $\mathbf{A} - \mathbf{B}$ is a positive semi-definite matrix.

Under the above conditions, the minimum rate of exponential convergence is $\frac{\lambda_{min}(\mathbf{\Gamma})}{2\sigma_2||\mathbf{X}||^2}$*, where* $\lambda_{min}(.)$ *denotes the minimum eigenvalue of a matrix and* σ_2 *is defined in* (5)*. If* $\mathbf{\Gamma} = 0$ *in* (29)*, the disturbance tracking error will converge asymptotically to zero.*

■

Proof. Consider the following candidate Lyapunov function:

$$\begin{aligned} W(\Delta\boldsymbol{\tau}_d, \mathbf{q}) &= \Delta\boldsymbol{\tau}_d^T \mathbf{X}^T \hat{\mathbf{M}}(\mathbf{q}) \mathbf{X} \Delta\boldsymbol{\tau}_d \\ &= (\mathbf{X}\Delta\boldsymbol{\tau}_d)^T \hat{\mathbf{M}}(\mathbf{q})(\mathbf{X}\Delta\boldsymbol{\tau}_d). \end{aligned} \tag{30}$$

Since $\hat{\mathbf{M}}(\mathbf{q})$ is symmetric and positive definite and the matrix $\mathbf{X}$ is invertible, the matrix $\mathbf{X}^T\hat{\mathbf{M}}(\mathbf{q})\mathbf{X}$ is also positive definite. Thus, the scalar function W is positive definite. Also, W is radially unbounded. Taking the time-derivative of W and using (26), (27) and (28) when $\dot{\boldsymbol{\tau}}_d \approx \mathbf{0}$, yields

$$\begin{aligned} &\dot{W}(\Delta\boldsymbol{\tau}_d, \mathbf{q}) = \Delta\dot{\boldsymbol{\tau}}_d^T \mathbf{X}^T \hat{\mathbf{M}}(\mathbf{q}) \mathbf{X} \Delta\boldsymbol{\tau}_d + \\ &\Delta\boldsymbol{\tau}_d^T \mathbf{X}^T \hat{\mathbf{M}}(\mathbf{q}) \mathbf{X} \Delta\dot{\boldsymbol{\tau}}_d + \Delta\boldsymbol{\tau}_d^T \mathbf{X}^T \dot{\hat{\mathbf{M}}}(\mathbf{q}) \mathbf{X} \Delta\boldsymbol{\tau}_d = \\ &-\Delta\boldsymbol{\tau}_d^T \hat{\mathbf{M}}^{-T}(\mathbf{q}) \mathbf{X}^{-T} \mathbf{X}^T \hat{\mathbf{M}}(\mathbf{q}) \mathbf{X} \Delta\boldsymbol{\tau}_d \\ &-\Delta\boldsymbol{\tau}_d^T \mathbf{X}^T \hat{\mathbf{M}}(\mathbf{q}) \mathbf{X} \mathbf{X}^{-1} \hat{\mathbf{M}}^{-1}(\mathbf{q}) \Delta\boldsymbol{\tau}_d \\ &+\Delta\boldsymbol{\tau}_d^T \mathbf{X}^T \dot{\hat{\mathbf{M}}}(\mathbf{q}) \mathbf{X} \Delta\boldsymbol{\tau}_d \Rightarrow \\ &\dot{W}(\Delta\boldsymbol{\tau}_d, \mathbf{q}) = -\Delta\boldsymbol{\tau}_d^T [\mathbf{X} + \mathbf{X}^T - \mathbf{X}^T \dot{\hat{\mathbf{M}}}(\mathbf{q}) \mathbf{X}] \Delta\boldsymbol{\tau}_d. \end{aligned} \tag{31}$$

According to Condition 2 and (31), $\dot{W}$ is negative definite for all $\Delta\boldsymbol{\tau}_d \in R^n$. Therefore, the disturbance tracking error asymptotically converges to zero: $\lim_{t\to\infty} \Delta\boldsymbol{\tau}_d = 0$ for all $\Delta\boldsymbol{\tau}_d \in R^n$.

Again consider the candidate Lyapunov function in (30). Condition 2 and (31) yield

$$\dot{W} \leq -\Delta\boldsymbol{\tau}_d^T \mathbf{\Gamma} \Delta\boldsymbol{\tau}_d, \ \ \forall \Delta\boldsymbol{\tau}_d \in R^n. \tag{32}$$

Therefore, the disturbance observer tracking error converges exponentially to zero for $\forall \Delta\boldsymbol{\tau}_d \in R^n$ when $\mathbf{\Gamma} \neq 0$.

On the other hand, using Rayleigh Inequality (see, for example, Theorem 2.5 in (Marquez, 2003)), it is observed that

$$\lambda_{min}(\mathbf{X}^T\hat{\mathbf{M}}(\mathbf{q})\mathbf{X})||\Delta\boldsymbol{\tau}_d||^2 \leq W \leq \\ \lambda_{max}(\mathbf{X}^T\hat{\mathbf{M}}(\mathbf{q})\mathbf{X})||\Delta\boldsymbol{\tau}_d||^2, \forall\Delta\boldsymbol{\tau}_d \in R^n. \tag{33}$$

Since $\mathbf{X}^T\hat{\mathbf{M}}(\mathbf{q})\mathbf{X}$ is a symmetric matrix, it can be seen that

$$\lambda_{max}(\mathbf{X}^T\hat{\mathbf{M}}(\mathbf{q})\mathbf{X}) = ||\mathbf{X}^T\hat{\mathbf{M}}(\mathbf{q})\mathbf{X}|| \leq \\ ||\mathbf{X}^T||.||\hat{\mathbf{M}}(\mathbf{q})||.||\mathbf{X}|| = ||\hat{\mathbf{M}}(\mathbf{q})||.||\mathbf{X}||^2. \tag{34}$$

So, $W \leq ||\hat{\mathbf{M}}(\mathbf{q})||.||\mathbf{X}||^2.||\Delta\boldsymbol{\tau}_d||^2$. According to (5), it can be observed that

$$W \leq \sigma_2||\mathbf{X}||^2.||\Delta\boldsymbol{\tau}_d||^2. \tag{35}$$

The above inequality results in $||\Delta\boldsymbol{\tau}_d||^2 \geq \frac{W}{\sigma_2||\mathbf{X}||^2}$. On the other hand, the Rayleigh Inequality along with (32) results in

$$\dot{W} \leq -\lambda_{min}(\boldsymbol{\Gamma})||\Delta\boldsymbol{\tau}_d||^2. \tag{36}$$

Also note that $\lambda_{min}(\boldsymbol{\Gamma}) > 0$ because $\boldsymbol{\Gamma}$ is positive definite. Therefore, from (36) and (35) it is seen that

$$\dot{W} \leq -\frac{\lambda_{min}(\boldsymbol{\Gamma})}{\sigma_2||\mathbf{X}||^2}W \Rightarrow W(t) \leq W(t_0)\exp[-\frac{\lambda_{min}(\boldsymbol{\Gamma})}{\sigma_2||\mathbf{X}||^2}t]. \tag{37}$$

Also, note that (5), (30) and Rayleigh Inequality yield

$$W \geq \sigma_1\Delta\boldsymbol{\tau}_d^T\mathbf{X}^T\mathbf{X}\Delta\boldsymbol{\tau}_d \\ \geq \sigma_1\lambda_{min}(\mathbf{X}^T\mathbf{X})||\Delta\boldsymbol{\tau}_d||^2. \tag{38}$$

From relations (37) and (38), it can be observed that

$$||\Delta\boldsymbol{\tau}_d||^2 \leq \frac{W(t_0)}{\sigma_1\lambda_{min}(\mathbf{X}^T\mathbf{X})}\exp[-\frac{\lambda_{min}(\boldsymbol{\Gamma})}{\sigma_2||\mathbf{X}||^2}t]. \tag{39}$$

Thus, the minimum convergence rate of the disturbance tracking error is $\frac{\lambda_{min}(\boldsymbol{\Gamma})}{2\sigma_2||\mathbf{X}||^2}$. □

Having addressed the case of slow-varying disturbances, now the case

where the robot is experiencing fast-varying disturbances is considered. The following theorem addresses the case where the robotic manipulator is subject to fast-varying disturbances.

Theorem 2. *Consider the robotic manipulator subject to disturbances described by* (15)*. The disturbance observer is given in* (25) *with the disturbance observer gain matrix* $\mathbf{L}(\mathbf{q})$ *defined in* (27) *and the disturbance observer auxiliary vector* $\mathbf{p}(\dot{\mathbf{q}})$ *defined in* (28)*. The disturbance tracking error* $\boldsymbol{\tau}_d$ *is globally uniformly ultimately bounded if:*

- *The first two conditions of the Theorem 1 hold,*
- *The rate of change of the lumped disturbance is bounded, i.e.,* $\exists \kappa > 0$ *such that* $||\dot{\boldsymbol{\tau}}_d(t)|| \leq \kappa$ *for all* $t > 0$*.*

Under the above conditions and for all $\Delta\boldsymbol{\tau}_d(0) \in R^n$*, the tracking error converges with an exponential rate, equal to* $\frac{(1-\theta)\lambda_{min}(\mathbf{\Gamma})}{2\sigma_2||\mathbf{X}||^2}$*, to the ball with radius* $\frac{2\kappa\sigma_2||\mathbf{X}||^2}{\theta\lambda_{min}(\mathbf{\Gamma})}$ *where* $0 < \theta < 1$*.*

■

Proof. Again, consider the Lyapunov Candidate function in (30). According to (35) and (38), it is seen that

$$\sigma_1\lambda_{min}(\mathbf{X}^T\mathbf{X})||\Delta\boldsymbol{\tau}_d||^2 \leq W \leq \sigma_2||\mathbf{X}||^2||\Delta\boldsymbol{\tau}_d||^2. \tag{40}$$

Note that W is a positive definite and radially unbounded function. Taking the time derivative of the Lyapunov function and using (26), it is observed that

$$\begin{aligned}\dot{W}(\Delta\boldsymbol{\tau}_d, \mathbf{q}) &= -\Delta\boldsymbol{\tau}_d^T[\mathbf{X} + \mathbf{X}^T - \mathbf{X}^T\dot{\hat{\mathbf{M}}}(\mathbf{q})\mathbf{X}]\Delta\boldsymbol{\tau}_d \\ &+\dot{\boldsymbol{\tau}}_d^T\mathbf{X}^T\hat{\mathbf{M}}(\mathbf{q})\mathbf{X}\Delta\boldsymbol{\tau}_d + \Delta\boldsymbol{\tau}_d^T\mathbf{X}^T\hat{\mathbf{M}}(\mathbf{q})\mathbf{X}\dot{\boldsymbol{\tau}}_d.\end{aligned} \tag{41}$$

On the other hand, according to Schwartz Inequality and (5) and since $||\dot{\boldsymbol{\tau}}_d(t)|| \leq \kappa$, it is seen that

$$\dot{\boldsymbol{\tau}}_d^T\mathbf{X}^T\hat{\mathbf{M}}(\mathbf{q})\mathbf{X}\Delta\boldsymbol{\tau}_d \leq \kappa\sigma_2||\mathbf{X}||^2||\Delta\boldsymbol{\tau}_d||. \tag{42}$$

Using the inequality (29) and (41), it can be observed that

$$\begin{aligned}
&\dot{W} \leq -\lambda_{min}(\mathbf{\Gamma})||\Delta\boldsymbol{\tau}_d||^2 + 2\kappa\sigma_2||\mathbf{X}||^2||\Delta\boldsymbol{\tau}_d|| \\
&= -(1-\theta)\lambda_{min}(\mathbf{\Gamma})||\Delta\boldsymbol{\tau}_d||^2 - \theta\lambda_{min}(\mathbf{\Gamma})||\Delta\boldsymbol{\tau}_d||^2 \\
&+2\kappa\sigma_2||\mathbf{X}||^2||\Delta\boldsymbol{\tau}_d||, \qquad (43)
\end{aligned}$$

where $\theta \in (0,1)$. Therefore,

$$\dot{W} \leq -(1-\theta)\lambda_{min}(\mathbf{\Gamma})||\Delta\boldsymbol{\tau}_d||^2, \forall||\Delta\boldsymbol{\tau}_d|| \geq \frac{2\kappa\sigma_2||\mathbf{X}||^2}{\theta\lambda_{min}(\mathbf{\Gamma})}. \qquad (44)$$

According to (40), (44) and the uniform ultimate boundedness theorems (see, for example, Theorem 5.1 and Corollary 5.1 in (Khalil, 1996)), it can be seen that the tracking error is globally uniformly ultimately bounded. Similar to (37), it can be observed that

$$\begin{aligned}
&\dot{W} \leq -\frac{(1-\theta)\lambda_{min}(\mathbf{\Gamma})}{\sigma_2||\mathbf{X}||^2}W \Rightarrow \\
&W(t) \leq W(t_0)\exp[-\frac{(1-\theta)\lambda_{min}(\mathbf{\Gamma})}{\sigma_2||\mathbf{X}||^2}t], \\
&\forall||\Delta\boldsymbol{\tau}_d|| \geq \frac{2\kappa\sigma_2||\mathbf{X}||^2}{\theta\lambda_{min}(\mathbf{\Gamma})}. \qquad (45)
\end{aligned}$$

From (40) and (45), it is seen that

$$\begin{aligned}
&||\Delta\boldsymbol{\tau}_d||^2 \leq \frac{W(t_0)}{\sigma_1\lambda_{min}(\mathbf{X}^T\mathbf{X})}\exp[-\frac{(1-\theta)\lambda_{min}(\mathbf{\Gamma})}{\sigma_2||\mathbf{X}||^2}t], \\
&\forall||\Delta\boldsymbol{\tau}_d|| \geq \frac{2\kappa\sigma_2||\mathbf{X}||^2}{\theta\lambda_{min}(\mathbf{\Gamma})}. \qquad (46)
\end{aligned}$$

Therefore,

$$\begin{aligned}
&||\Delta\boldsymbol{\tau}_d(t)|| \leq \sqrt{\frac{W(t_0)}{\sigma_1\lambda_{min}(\mathbf{X}^T\mathbf{X})}}\exp[-\frac{(1-\theta)\lambda_{min}(\mathbf{\Gamma})}{2\sigma_2||\mathbf{X}||^2}t] \\
&+\frac{2\kappa\sigma_2||\mathbf{X}||^2}{\theta\lambda_{min}(\mathbf{\Gamma})}, \forall t \geq 0. \qquad (47)
\end{aligned}$$

Therefore, the tracking error converges with an exponential rate, equal to $\frac{(1-\theta)\lambda_{min}(\mathbf{\Gamma})}{2\sigma_2||\mathbf{X}||^2}$ to the ball with radius $\frac{2\kappa\sigma_2||\mathbf{X}||^2}{\theta\lambda_{min}(\mathbf{\Gamma})}$ where $0 < \theta < 1$ for all $\Delta\boldsymbol{\tau}_d(0) \in R^n$.

□

Remark. Conventional linear disturbance observers and nonlinear disturbance observers proposed by (Chen et al., 2000) and (Nikoobin and Haghighi, 2009) are special cases of the disturbance observer in (25), disturbance observer gain matrix (27), and disturbance observer auxiliary vector (28) in the following ways:

- In the conventional linear disturbance observers (Ohnishi et al., 1996) the robot inertia matrix estimate $\hat{\mathbf{M}}(\mathbf{q})$ is represented by a constant diagonal matrix of the form $\mathbf{diag}\{m_i\}$ where $m_i > 0,\ i = 1, \ldots, n$ are positive real constants. Also, the vector $\hat{\mathbf{N}}(\mathbf{q}, \dot{\mathbf{q}})$ is chosen to be zero and the matrix $\mathbf{X}$ is taken to be a constant diagonal matrix $\mathbf{diag}\{x_i\}$ with $x_i > 0$.

- In (Chen et al., 2000) and (Nikoobin and Haghighi, 2009), the nonlinear disturbance observer design problem was solved for a serial planar robot with 2 and n revolute joints, respectively. In both of these, it was assumed that the exact dynamic model of the robotic manipulator is available, i.e., they took $\hat{\mathbf{M}}(\mathbf{q}) = \mathbf{M}(\mathbf{q})$ and $\hat{\mathbf{N}}(\mathbf{q}, \dot{\mathbf{q}}) = \mathbf{N}(\mathbf{q}, \dot{\mathbf{q}})$. Also, the vector $\mathbf{p}(\mathbf{q}, \dot{\mathbf{q}})$ was considered to be

$$\mathbf{p}(\dot{\mathbf{q}}) = c \begin{bmatrix} \dot{q}_1 \\ \dot{q}_1 + \dot{q}_2 \\ \vdots \\ \dot{q}_1 + \dot{q}_2 + \cdots + \dot{q}_n \end{bmatrix}. \tag{48}$$

  This is clearly a special case of the proposed vector $\mathbf{p}(\dot{\mathbf{q}})$ in (28), when $\mathbf{X}^{-1}$ is chosen to be

$$\mathbf{X}^{-1} = c \begin{bmatrix} 1 & 0 & \ldots & 0 \\ 1 & 1 & \ddots & \vdots \\ \vdots & \vdots & \ddots & 0 \\ 1 & 1 & \ldots & 1 \end{bmatrix}. \tag{49}$$

Also, note that Nikoobin et al. and Chen et al. had to rely on the special structure of mass matrices of planar serial manipulators in order to determine the constant c. In other words, the constant c cannot be determined if the manipulator is nonplanar using methods proposed in (Chen et al., 2000; Nikoobin and Haghighi, 2009).

$\diamondsuit$

3.2. LMI formulation of the design method

According to Theorems 1 and 2, the disturbance observer design problem reduces to finding a constant invertible matrix $\mathbf{X}$ such that the inequality (29) is satisfied. The following theorem shows how (29) can be formulated as a linear matrix inequality.

Theorem 3. *Define the matrix* $\mathbf{Y} = \mathbf{X}^{-1}$ *and assume that an upper bound of* $||\dot{\hat{\mathbf{M}}}(\mathbf{q})||$ *is* ζ*. The inequality* (29) *holds if the following LMI is satisfied:*

$$\begin{bmatrix} \mathbf{Y} + \mathbf{Y}^T - \zeta\mathbf{I} & \mathbf{Y}^T \\ \mathbf{Y} & \mathbf{\Gamma}^{-1} \end{bmatrix} \geq 0. \tag{50}$$

Proof. Multiply (29) by $\mathbf{Y}$ and $\mathbf{Y}^T$ from right and left, respectively to get

$$\mathbf{Y} + \mathbf{Y}^T - \mathbf{Y}^T\mathbf{\Gamma}\mathbf{Y} \geq \dot{\hat{\mathbf{M}}}(\mathbf{q}). \tag{51}$$

Since $||\dot{\hat{\mathbf{M}}}(\mathbf{q})|| \leq \zeta$, it is observed that $\zeta\mathbf{I} \geq \dot{\hat{\mathbf{M}}}(\mathbf{q})$ where $\mathbf{I}$ is the identity matrix. Therefore, (51) holds if

$$\mathbf{Y} + \mathbf{Y}^T - \mathbf{Y}^T\mathbf{\Gamma}\mathbf{Y} \geq \zeta\mathbf{I}. \tag{52}$$

The above inequality is equivalent to $\mathbf{Y} + \mathbf{Y}^T - \zeta\mathbf{I} - \mathbf{Y}^T\mathbf{\Gamma}\mathbf{Y} \geq 0$. Note that $\mathbf{\Gamma}$ is a positive definite matrix. According to the Schur Complement Inequality (refer to the Appendix A), this inequality holds if and only if the LMI (50) holds. □

Note that LMI software packages have the ability to solve (50) simultaneously for $\mathbf{Y}$ and $\mathbf{\Gamma}$ when $\mathbf{\Gamma}$ is not known.

4. Practical considerations in the design of disturbance observers

In this section, practical issues in the design of disturbance observers are addressed. Also, an analytical solution to the observer design problem will be proposed.

4.1. Rate of convergence of the disturbance observer and the sensitivity to measurement noise

As it was seen in Theorems 1 and 2, the rate of convergence of the tracking error is proportional to $\frac{1}{||\mathbf{Y}^{-1}||^2}$, where $\mathbf{X}^{-1} = \mathbf{Y}$. Also, the radius of the ball that the tracking errors converge to, in the case of fast-varying disturbances, is proportional to $||\mathbf{Y}^{-1}||^2$ (see Theorem 2). Since a smaller $||\mathbf{Y}^{-1}||$ implies a larger disturbance observer gain $||\mathbf{L}||$ due to (27), a large observer gain is needed in order to increase the rate of convergence and the accuracy of the disturbance observer. On the other hand, large disturbance observer gains will increase the sensitivity of the observer to measurement noise by amplifying this noise. From this perspective, it is desirable to choose the disturbance observer gain $||\mathbf{L}||$ to be small. Thus, there exists a trade-off between the rate of convergence and the accuracy of the estimations and the noise amplification. According to (27), it can be seen that

$$||\mathbf{L}|| \leq ||\mathbf{Y}||.||\hat{\mathbf{M}}^{-1}(\mathbf{q})||. \tag{53}$$

Since the disturbance observer gain directly depends on the matrix $\mathbf{Y}$, this matrix cannot be chosen to be very large. Assume that it is required to limit the matrix $\mathbf{Y}$ to $\nu\mathbf{I}$ to reduce the noise amplification. Then, the following set of LMIs needs to be solved:

$$\begin{aligned} \begin{bmatrix} \mathbf{Y} + \mathbf{Y}^T - \zeta\mathbf{I} & \mathbf{Y}^T \\ \mathbf{Y} & \mathbf{\Gamma}^{-1} \end{bmatrix} &\geq 0, \\ \mathbf{Y} &\leq \nu\mathbf{I}. \end{aligned} \tag{54}$$

LMI software packages such as MATLAB LMI Control Toolbox have the ability to solve a set of LMIs, such as the one in (54), simultaneously (Gahinet et al., 1995).

4.2. Analytical solution to the disturbance observer design problem

When the matrix $\mathbf{Y}$ is chosen to be $y\mathbf{I}$ [3], where $\mathbf{I}$ is the identity matrix, the LMI used for observer design in (50) will have an explicit analytical solution. Assume that it is desired that the minimum convergence rate of

[3] Note that the matrix $\mathbf{Y}$ is a diagonal matrix with equal elements on its diagonal. The units of these diagonal elements are not necessarily the same. In fact, if the i^{th} joint of the robot is revolute (prismatic) the unit of the i^{th} element will be $\frac{rad}{sec}$ ($\frac{m}{sec}$)).

the disturbance tracking error to be equal to β. Also assume that $\mathbf{\Gamma} = \gamma\mathbf{I}$. According to Theorem 1, it is seen that

$$\gamma = \frac{2\beta\sigma_2}{y^2}, \tag{55}$$

and, the LMI (50) turns into

$$\begin{bmatrix} (2y-\zeta)\mathbf{I} & y\mathbf{I} \\ y\mathbf{I} & \frac{y^2}{2\beta\sigma_2}\mathbf{I} \end{bmatrix} \geq 0. \tag{56}$$

According to Schur Complement Inequality, the above LMI is equivalent to

$$\begin{aligned} &(2y-\zeta)\mathbf{I} - (y\mathbf{I})^T(\frac{y^2}{2\beta\sigma_2}\mathbf{I})^{-1}(y\mathbf{I}) \geq 0 \\ &\Leftrightarrow (2y-\zeta-2\beta\sigma_2) \geq 0 \Leftrightarrow y \geq \frac{1}{2}\zeta + \beta\sigma_2. \end{aligned} \tag{57}$$

The above inequality clearly depicts the trade-off existing between the minimum convergence rate and the noise amplification. Note that ζ and σ_2 are constants and depend on the robot dynamic parameters and the maximum joint velocities of the robot. Faster convergence rates and better accuracy require larger values of β. This, in turn, means larger values of y and thus results in more sensitivity to noise. Since it is required to reduce the sensitivity to noise in disturbance rejection applications and at the same time guarantee the minimum convergence rate of tracking error to be equal to β, the matrix $\mathbf{Y}$ can be chosen to be

$$\mathbf{Y}_{optimal} = \frac{1}{2}(\zeta + 2\beta\sigma_2)\mathbf{I}. \tag{58}$$

Then, based on (27) and $\mathbf{X}^{-1} = \mathbf{Y}$, $\mathbf{L}$ is found.

5. Simulation Study

SCARA (Selective Compliance Assembly Robot Arm) is an industrial 4-DOF robotic arm, which is widely used in the assembly of electronic circuits and devices. The first two joints of the arm, which are used to generate motion in a horizontal plane, are revolute and have parallel axes of rotation. The third joint of the arm is a prismatic joint, which controls the vertical

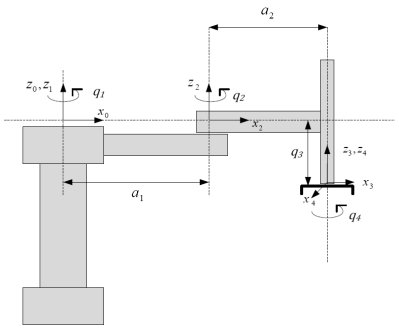

Figure 2: SCARA robotic arm.

motion (z-axis) of the end-effector. Finally, the last joint is revolute and is used to orient the gripper about the z-axis. Do not confuse this with the auxiliary vector of the disturbance observer given in (25). Figure 2 depicts a schematic diagram of this manipulator. The dynamics of the SCARA manipulator is (Voglewede et al., 2009):

$$\begin{aligned}
\mathbf{M}(\mathbf{q}) &= \begin{bmatrix} p_1 + p_2 c_2 & p_3 + 0.5 p_2 c_2 & 0 & -p_5 \\ p_3 + 0.5 p_2 c_2 & p_3 & 0 & -p_5 \\ 0 & 0 & p_4 & 0 \\ -p_5 & -p_5 & 0 & p_5 \end{bmatrix}, \\
\mathbf{C}(\mathbf{q}, \dot{\mathbf{q}}) &= \begin{bmatrix} -p_2 s_2 \dot{q}_2 & -0.5 p_2 s_2 \dot{q}_2 & 0 & 0 \\ 0.5 p_2 s_2 \dot{q}_1 & 0 & 0 & 0 \\ 0 & 0 & 0 & 0 \\ 0 & 0 & 0 & 0 \end{bmatrix}, \\
\mathbf{G}(\mathbf{q}) &= \begin{bmatrix} 0 \\ 0 \\ -p_4 g \\ 0 \end{bmatrix}.
\end{aligned} \tag{59}$$

The SCARA arm parameters are defined as

$$
\begin{aligned}
p_1 &= \sum_{i=1}^{4} I_i + m_1 x_1^2 + m_2(x_2^2 + a_1^2) + \\
&\quad (m_3 + m_4)(a_1^2 + a_2^2), \\
p_2 &= 2a_1[x_2 m_2 + a_2(m_3 + m_4)], \\
p_3 &= \sum_{i=2}^{4} I_i + m_2 x_2^2 + a_2^2(m_3 + m_4), \\
p_4 &= m_3 + m_4, \\
p_5 &= I_4,
\end{aligned} \tag{60}
$$

where I_i is the moment of inertia around the centroid, m_i is the mass, x_i is the mass center, and a_i is the length for link i. The Jacobian of the SCARA manipulator, with respect to the robot base frame, is (Liu et al., 2009):

$$
\mathbf{J}(\mathbf{q}) = \begin{bmatrix} -a_1 s_1 - a_2 s_{12} & -a_2 s_{12} & 0 & 0 \\ a_1 c_1 + a_2 c_{12} & a_2 c_{12} & 0 & 0 \\ 0 & 0 & -1 & 0 \\ 1 & 1 & 0 & 1 \end{bmatrix}. \tag{61}
$$

In the above, $s_2 = \sin(q_2)$, $c_2 = \cos(q_2)$, $s_{12} = \sin(q_1 + q_2)$, $c_{12} = \cos(q_1 + q_2)$

Two types of disturbances are exerted to the robot, namely friction and external payload. Computed-torque scheme is adopted for position control (Spong et al., 2005):

$$
\begin{aligned}
&\boldsymbol{\tau} = \mathbf{M}(\mathbf{q})\{\ddot{\mathbf{q}}_{ref} + \mathbf{K}_v(\dot{\mathbf{q}}_{ref} - \dot{\mathbf{q}}) + \mathbf{K}_p(\mathbf{q}_{ref} - \mathbf{q})\} \\
&+\mathbf{C}(\mathbf{q}, \dot{\mathbf{q}})\dot{\mathbf{q}} + \mathbf{G}(\mathbf{q}).
\end{aligned} \tag{62}
$$

Figure 3 depicts the computed-torque controller and the disturbance observer that is used for disturbance rejection. The vector $\boldsymbol{\tau}_d$ represents the lumped disturbance, which deteriorates the tracking performance of the robot control system. The disturbance observer role is to estimate this disturbance as closely as possible. The estimated disturbance $\hat{\boldsymbol{\tau}}_d$ is then subtracted from the control signal $\boldsymbol{\tau}$ to cancel out or minimize the effect of the disturbance.

Note that $\mathbf{q}_{ref}$ is the vector of desired joint positions as a function of time. The external end-effector payload is chosen to be a weight exerted to the

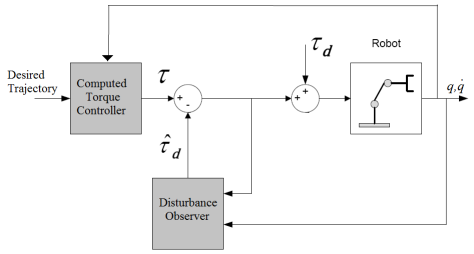

Figure 3: Disturbance observer used for disturbance rejection.

Parameter	Value	Parameter	Value
m_1	15 kg	m_2	12 kg
m_3	3 kg	m_4	3 kg
I_1	$0.02087m_1$ kg.m^2	I_2	$0.08m_2$ kg.m^2
I_3	0.05 kg.m^2	I_4	$0.02m_4$ kg.m^2
a_1	0.5 m	a_2	0.4 m
x_1	0.25 m	x_2	0.2 m
F_{c1}	0.49 N.m	F_{c2}	0.31 N.m
F_{c3}	0.1 N	F_{c4}	0.1 N.m
F_{s1}	3.5 N.m	F_{s2}	2.8 N.m
F_{s3}	1.65 N	F_{s4}	0.7 N.m
F_{v1}	0.15 $\frac{kg.m}{s}$	F_{v2}	0.12 $\frac{kg.m}{s}$
F_{v3}	0.08 $\frac{kg}{s}$	F_{v4}	0.03 $\frac{kg.m}{s}$
v_{s1}	0.19 $\frac{rad}{s}$	v_{s2}	0.15 $\frac{rad}{s}$
v_{s3}	0.12 $\frac{m}{s}$	v_{s4}	0.03 $\frac{rad}{s}$
$\mathbf{K}_v$	$1.5\mathbf{I}$	$\mathbf{K}_p$	$2\mathbf{I}$
$\mathbf{Y} = \mathbf{X}^{-1}$	$95.8\mathbf{I}$	g	9.8 $\frac{N}{kg}$

Table 2: Simulation parameters

robot end-effector in the z direction. This weight is equal to 2N. The friction torques acting on the joints of the robots are generated based on the model in (Kermani et al., 2007), (Armstrong-Hélouvry et al., 1994). For the $i-th$ joint of the robot, $i = 1, 2, 3, 4$, the friction is modelled as

$$\begin{aligned} \tau_{i_{friction}} &= F_{ci}\text{sgn}(\dot{q}_i)[1 - \exp(\frac{-\dot{q}_i^2}{v_{si}^2})] \\ &\quad + F_{si}\text{sgn}(\dot{q}_i)\exp(\frac{-\dot{q}_i^2}{v_{si}^2}) + F_{vi}\dot{q}_i \end{aligned} \tag{63}$$

where F_{ci}, F_{si}, F_{vi} are the Coulomb, static, and viscous friction coefficients, respectively. The parameter v_{si} is the Stribeck parameter. Table 2 gives the simulation parameters.

The total disturbance vector acting on the joints of the robot can be computed by

$$\boldsymbol{\tau}_d = \boldsymbol{\tau}_{friction} + \mathbf{J}^T \mathbf{F}_{payload}. \tag{64}$$

Now, simulations are performed for a generic pick-and-place maneuver [4]. In this class of maneuvers the robotic arm starts from rest, accelerates slowly and eventually decelerates to stop (Damaren and Sharf, 1995). The reference trajectory provided for the joints of the robot is parametrized by

$$\theta_n(t) = \theta_{dn}(\frac{t}{T} - \frac{1}{2\pi}\sin(\frac{2\pi t}{T})),\ 0 \leq t \leq T,\ 1 \leq n \leq 4, \tag{65}$$

where T is the duration time of the maneuver. In the simulations, the final joint positions are $\theta_{d1} = \frac{\pi}{5}$ rad, $\theta_{d2} = \frac{\pi}{8}$ rad, $\theta_{d3} = 1$ cm, $\theta_{d4} = \frac{\pi}{6}$ rad, and $T = 10$ sec. In the first case, no disturbance observer is used with the computed torque controller. In the second and the third cases, the disturbance observer proposed by Liu & Peng (Liu and Peng, 2000) and the disturbance observer proposed by the authors are used to estimate and suppress the joint frictions and the external payload together with computed torque law, respectively. In the disturbance observer proposed by Liu & Peng, the observer gain is chosen to be $K = \text{diag}\{11.60, 38.17, 23.95, 159.67\}$. The designed observer by the authors has a structure given by (25), (27) and (28). The matrix $\mathbf{Y} = \mathbf{X}^{-1} = y\mathbf{I}$ is chosen for designing the disturbance observer. Based on the parameters provided in Table 2, it is seen that

$$||\mathbf{M}(\mathbf{q})|| \leq 15. \tag{66}$$

By (17), the relation $\sigma_2 = 15$ holds. Eigenvalues of the matrix $\dot{\mathbf{M}}(\mathbf{q})$ are 0, 0, $\frac{1}{2}(-1+\sqrt{2})p_2\dot{q}_2\sin(q_2)$ and $\frac{1}{2}(-1-\sqrt{2})p_2\dot{q}_2\sin(q_2)$, respectively. It can be seen that

$$||\dot{\mathbf{M}}(\mathbf{q})|| \leq \frac{1}{2}(1+\sqrt{2})p_2\dot{q}_{2max} = 5.8\dot{q}_{2max}. \tag{67}$$

By Theorem 3, the parameter ζ is chosen to be $5.8\dot{q}_{2max}$. Assuming the

[4] It is expected that the Stribeck effect to be dominant in the beginning and the end of the pick-and-place maneuver; because, the robot accelerates from rest in the beginning of the maneuver and decelerates to stop in the end of the maneuver.

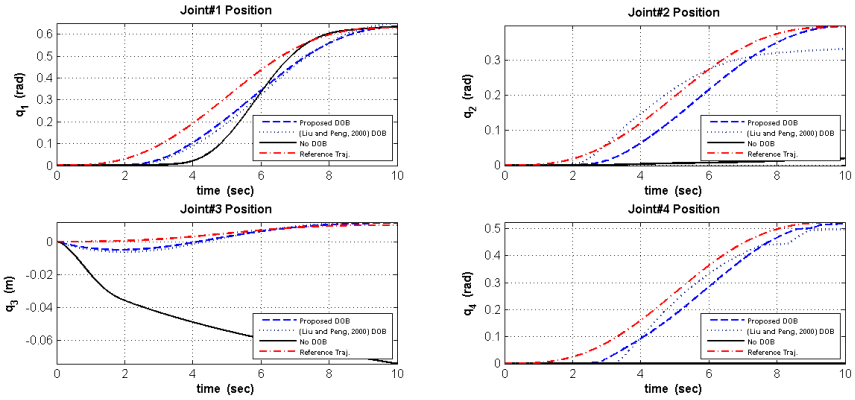

Figure 4: Simulation study: position of the joints of the SCARA robot.

	No DOB	(Liu and Peng, 2000) DOB	Proposed DOB
RMS Error Joint 1	9.11×10^{-2}	3.70×10^{-2}	3.39×10^{-2}
RMS Error Joint 2	2.38×10^{-1}	3.06×10^{-2}	2.14×10^{-2}
RMS Error Joint 3	5.92×10^{-2}	4.91×10^{-3}	3.89×10^{-3}
RMS Error Joint 4	3.29×10^{-1}	3.51×10^{-2}	2.87×10^{-2}

Table 3: Simulation study: Joint tracking error RMS values

maximum velocity of the second joint to be $\dot{q}_{2max} = 2\frac{rad}{sec}$ and the minimum convergence rate to be $\beta = 6$ and according to (58), it is seen that

$$\mathbf{Y}_{optimal} = \frac{1}{2}(5.8\dot{q}_{2max} + 2\beta\sigma_2) \Rightarrow \mathbf{Y}_{optimal} = 95.8\mathbf{I}. \tag{68}$$

Figures 4 and 5 illustrate the time profiles of the positions of the joints and position tracking errors of the robot, respectively. Table 3 contains the RMS values of joint tracking errors. As it can be observed, the computed-torque control law fails to track the position commands accurately when no disturbance observer is used. On the other hand, the position tracking errors are decreased when disturbance observers are used. Figures 6 and 7 depict the actual and estimated disturbances and disturbance tracking errors, respectively. Table 4 contains the RMS values of disturbance tracking errors. The disturbance and position tracking performance of the proposed disturbance observer excels the performance of that of proposed by (Liu and Peng, 2000).

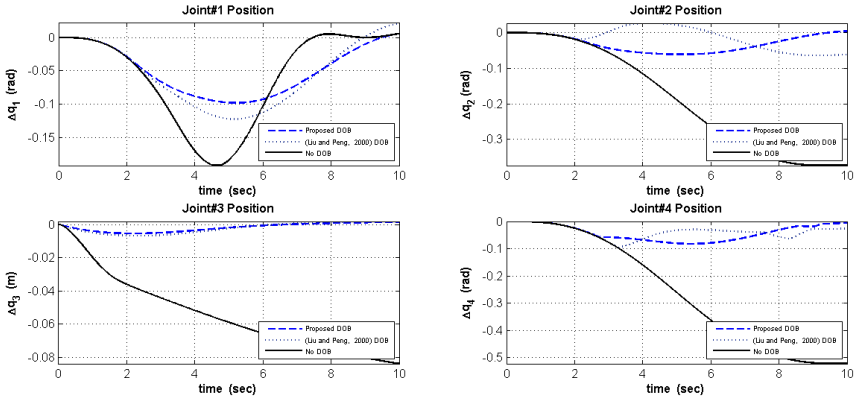

Figure 5: Simulation study: position tracking error time profiles.

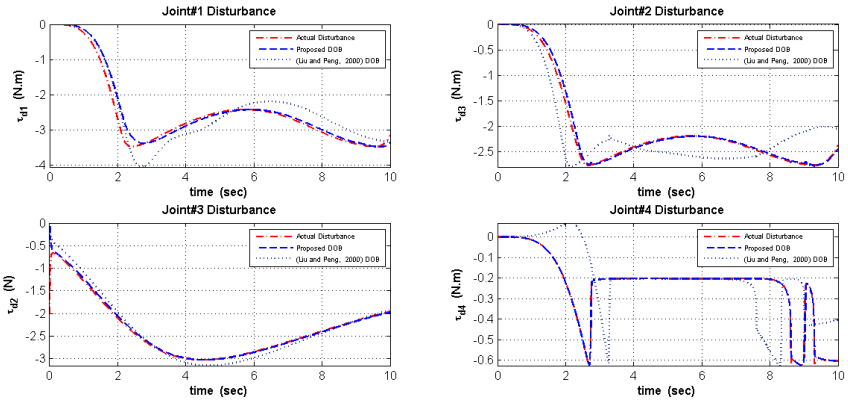

Figure 6: Simulation study: disturbance tracking time profiles.

	(Liu and Peng, 2000) DOB	Proposed DOB
RMS Error Joint 1	2.85×10^{-1}	2.68×10^{-1}
RMS Error Joint 2	1.61×10^{-1}	1.08×10^{-1}
RMS Error Joint 3	9.74×10^{-2}	9.63×10^{-2}
RMS Error Joint 4	1.31×10^{-2}	4.61×10^{-3}

Table 4: Simulation study: Disturbance tracking error RMS values

6. Experiments

The PHANToM Omni® (SensAble Technologies Inc., MA, USA) is a haptic device that can be used for a variety of purposes including virtual reality and teleoperation applications. The PHANToM Omni has three actu-

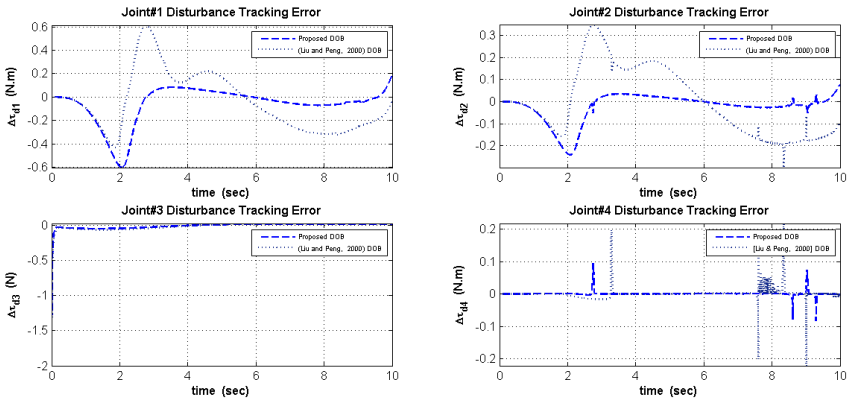

Figure 7: Simulation study: Disturbance tracking error time profiles.

ated revolute joints which provide the user with force feedback information. In addition to the actuated joints, the PHANToM robot has 3 wrist joints that are passive. The first and the third actuated joints of the PHANToM robot in experiments will be used while the second actuated joint is locked at 0^{deg}. Note that this mechanism is not confined to a constant 2-D plane and moves in three-dimensional space. Therefore, the nonlinear disturbance observer gain proposed by (Chen et al., 2000) or (Nikoobin and Haghighi, 2009) cannot be employed here. Figure 8 shows the PHANToM Omni setup that is used in the experiments. The PHANToM Omni is connected to the computer through an IEEE 1394 port. The PHANToM Omni end-effector position and orientation data are collected at a frequency of 1000 Hz. The disturbance observer is used to estimate and compensate for the joint frictions and external payload. The payload is a metal cube which is attached to the gimbal of the robot. Note that $c_i = \cos(q_i)$, $s_i = \sin(q_i)$, $c_{2.i} = \cos(2q_i)$, and $s_{2.i} = \sin(2q_i)$. The inertia matrix of the PHANToM robot, assuming $q_2 = 0$, is (Naerum et al., 2008):

$$\mathbf{M}(\mathbf{q}) = \begin{bmatrix} \alpha_1 + \alpha_2 c_{2.3} + \alpha_3 s_{2.3} + \alpha_4 c_3 + \alpha_5 s_3 & 0 \\ 0 & \alpha_6 \end{bmatrix}, \tag{69}$$

and defining

$$\mathbf{V}(\mathbf{q}, \dot{\mathbf{q}}) = [V_1, V_2]^T = \mathbf{C}(\mathbf{q}, \dot{\mathbf{q}})\dot{\mathbf{q}} + \mathbf{G}(\mathbf{q}), \tag{70}$$

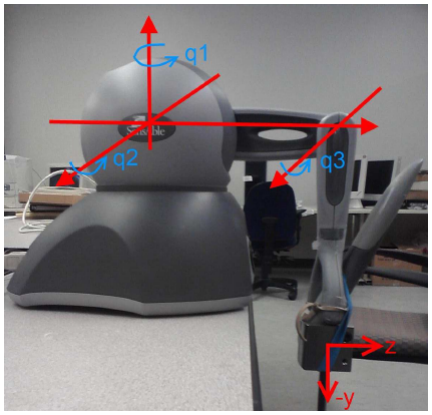

Figure 8: Experimental study: the PHANToM Omni hatpic device.

where the vector $\mathbf{V}(\mathbf{q}, \dot{\mathbf{q}})$ is the sum of the Coriolis, centrifugal and gravity forces, it is seen that

$$\begin{aligned} V_1 &= -2\alpha_2 \dot{q}_1 \dot{q}_3 \sin(2q_3) + 2\alpha_3 \dot{q}_1 \dot{q}_3 \cos(2q_3) \\ &\quad +\alpha_4 \dot{q}_1 \dot{q}_3 \cos(q_3) - \alpha_5 \dot{q}_1 \dot{q}_3 \sin(q_3), \\ V_2 &= 2\alpha_2 \dot{q}_1^2 \cos(q_3)\sin(q_3) - \alpha_3 \dot{q}_1^2 \cos(2q_3) - \\ &\quad \frac{1}{2}\alpha_4 \dot{q}_1^2 \cos(q_3) + \frac{1}{2}\alpha_5 \dot{q}_1^2 \sin(q_3) \\ &\quad +\alpha_7 \sin(q_3) + \alpha_8 \cos(q_3). \end{aligned} \tag{71}$$

The Jacobian of the PHANToM, considering $q_2 = 0$, is (Naerum et al., 2008):

$$\mathbf{J}(\mathbf{q}) = \begin{bmatrix} l_1 + l_2 s(q_3) & 0 \\ 0 & l_1 s(q_3) \end{bmatrix}, \tag{72}$$

where $l_1 = l_2 = 135^{mm}$ are the lengths of the first and the second link of the robot. Therefore, the disturbance due to the external payload which is being exerted to the first and the third joints of the robot is:

$$\boldsymbol{\tau}_{payload} = \mathbf{J}^T \mathbf{F} = \mathbf{J}^T \begin{bmatrix} 0 \\ mg \end{bmatrix} = \begin{bmatrix} 0 \\ mgl_1 s(q_3) \end{bmatrix}. \tag{73}$$

Parameter	Value	Parameter	Value
α_1	$6.11 \times 10^{-3} \pm 0.9 \times 10^{-3}$	α_2	$-2.89 \times 10^{-3} \pm 0.43 \times 10^{-3}$
α_3	$-4.24 \times 10^{-3} \pm 1.01 \times 10^{-3}$	α_4	$3.01 \times 10^{-3} \pm 0.52 \times 10^{-3}$
α_5	$2.05 \times 10^{-3} \pm 0.15 \times 10^{-3}$	α_6	$1.92 \times 10^{-3} \pm 0.23 \times 10^{-3}$
α_7	$1.60 \times 10^{-1} \pm 0.05 \times 10^{-1}$	α_8	$-8.32 \times 10^{-3} \pm 2.78 \times 10^{-3}$

Table 5: PHANToM Omni identified parameters

First, the PHANToM parameters were identified (refer to Appendix B). Table 5 gives the PHANToM Omni identified parameters. Based on the provided parameters and assuming $\dot{q}_{3max} = 1\frac{rad}{sec}$, it is seen that

$$||\hat{\mathbf{M}}(\mathbf{q})|| \leq 0.0132, \tag{74}$$

and,

$$||\dot{\hat{\mathbf{M}}}(\mathbf{q})|| \leq 0.0138. \tag{75}$$

By (17), the parameter σ_2 is chosen to be 0.0132. By Theorem 3, the relation $\zeta = 0.0138\dot{q}_{2max}$ holds. Assuming a minimum convergence rate of $\beta = 1$ and according to (58), it is observed that

$$\mathbf{Y}_{optimal} = \frac{1}{2}(0.0138 + 2 \times 0.0132 \times \beta) \Rightarrow \mathbf{Y}_{optimal} = 0.02\mathbf{I}. \tag{76}$$

Sinusoidal commands are supplied as the reference trajectory for the first and the third joints of the robot in the presence of the computed-torque control scheme (62). The experiments are performed in three different cases, namely, with no DOB, with the DOB proposed by (Liu and Peng, 2000), and with the DOB proposed in the paper. The proportional and derivative gains are chosen to be equal to $1.4\mathbf{I}$ and $0.5\mathbf{I}$, respectively. The DOB gain matrix of Liu & Peng observer has been chosen to be $\mathbf{I}$. In addition, the disturbance tracking performance of the proposed DOB is compared in the paper with that of employed by Katsura et al. (Katsura et al., 2003)[5] and Liu & Peng (Liu and Peng, 2000). The parameters of DOB of Katsura et al. have been chosen to be $g_{reac} = 100$ and $K_{tn} = 1$. Figures 9, 10, 11, and 12 illustrate the time profiles of positions and tracking errors of joints 1 and 3, respectively. Table 6 contains the RMS values of joint tracking errors. Figures 13 and 14

[5]This is the conventional linear disturbance observer that has been employed in numerous robotic applications. See, for example, (Natori et al., 2006, 2010; Katsura et al., 2010).

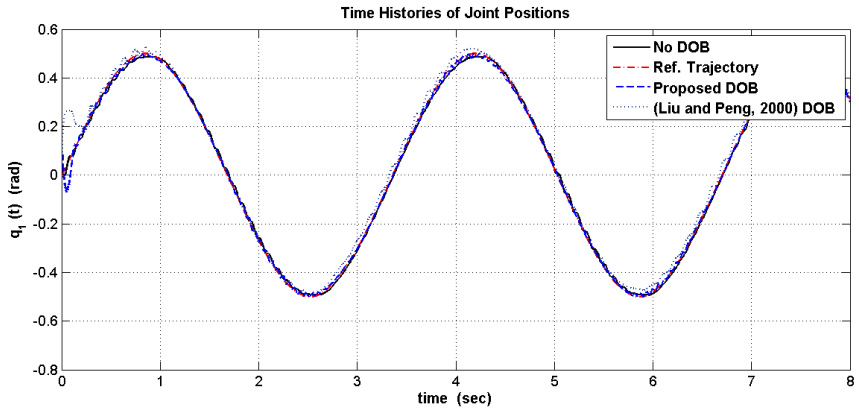

Figure 9: Experimental study: time profile of position of the first joint of the PHANToM robot.

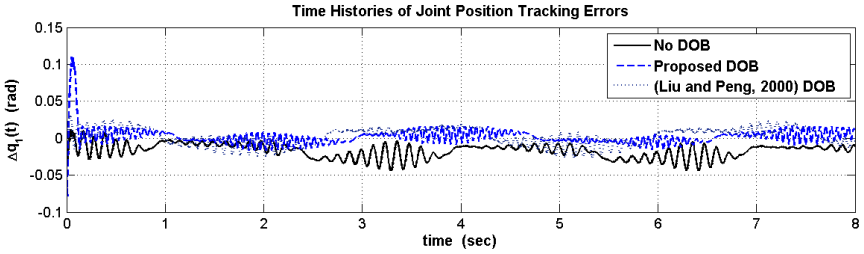

Figure 10: Experimental study: time profile of position tracking error of the first joint of the PHANToM robot.

	No DOB	(Liu and Peng, 2000) DOB	Proposed DOB
RMS Error Joint 1	2.02×10^{-2}	1.19×10^{-2}	9.98×10^{-3}
RMS Error Joint 3	1.23×10^{-1}	7.69×10^{-2}	3.31×10^{-2}

Table 6: experimental study: position tracking error RMS values

illustrate the time profiles of disturbances and disturbance tracking errors of joints 1 and 3, respectively. Table 7 contains the RMS values of disturbance tracking errors. Note that the identification of the dynamic model of the robot was not perfect. Therefore, dynamic uncertainties exist in the model of the robot. According to Theorem 2, the tracking error is guaranteed to be bounded and to converge to its ultimate bound region with an exponential rate. The disturbance and position tracking performance of the proposed disturbance observer excels the performance of that of proposed by (Liu and Peng, 2000) and (Katsura et al., 2003).

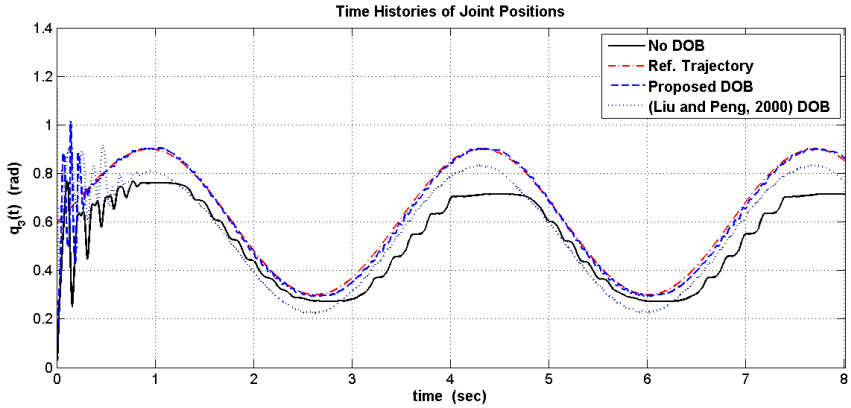

Figure 11: Experimental study: time profile of position of the third joint of the PHANToM robot.

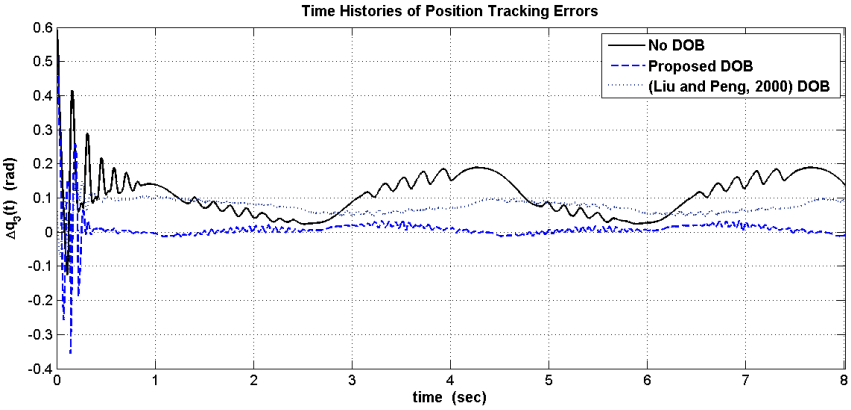

Figure 12: Experimental study: time profile of position tracking error of the third joint of the PHANToM robot.

	(Liu and Peng, 2000) DOB	(Katsura et al., 2003) DOB	Proposed DOB
RMS Error Joint 1	9.85×10^{-3}	1.44×10^{-2}	5.52×10^{-3}
RMS Error Joint 3	1.42×10^{-2}	2.02×10^{-2}	1.00×10^{-2}

Table 7: Experimental study: Disturbance tracking error RMS values

7. Conclusion

A general systematic disturbance observer design method for serial robotic manipulators has been proposed in this paper. The previously proposed linear and nonlinear disturbance observers can be unified in this gen-

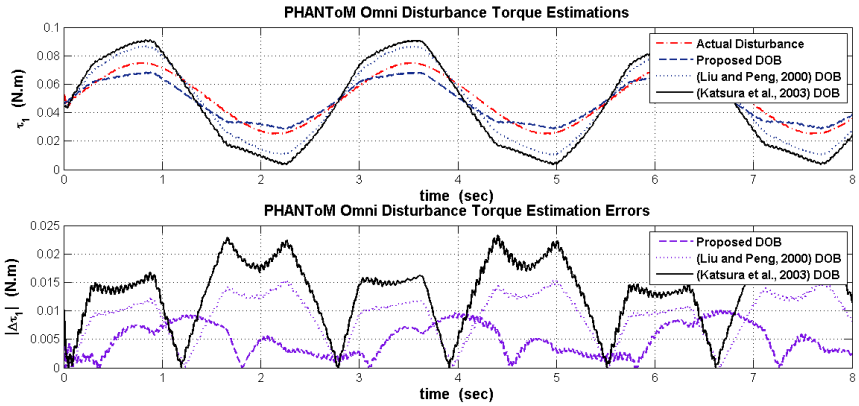

Figure 13: Experimental study: time profiles of disturbance tracking for the first joint of the PHANToM robot.

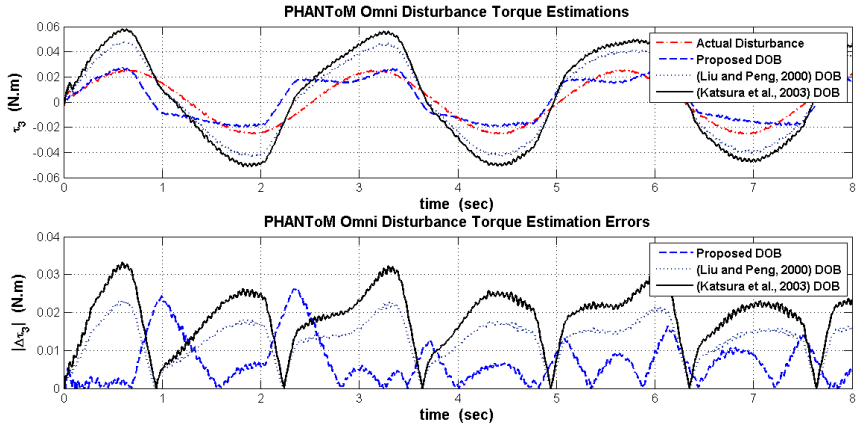

Figure 14: Experimental study: time profiles of disturbance tracking for the third joint of the PHANToM robot.

eral framework. Moreover, the proposed design method removes the previous restrictions on the number of degrees-of-freedom, the types of joints, and the manipulator configuration in the design of nonlinear disturbance observers. The observer design problem has been formulated as a linear matrix inequality (LMI). The proposed design method guarantees convergence of the observer tracking error to the origin with an exponential rate in the case of slow-varying disturbances. In the case of fast-varying disturbances, the tracking error is shown to be globally uniformly ultimately bounded. The trade-off between the rate of convergence of the tracking error

and the sensitivity to measurement noise has been discussed. In addition to the LMI formulation of the design problem, an analytical solution has been proposed. Simulations using an industrial manipulator and experiments involving a haptics-capable robot were presented to verify the effectiveness of the proposed approach.

Appendix A. Schur Complement Inequality

Schur Complement Inequality. *(Gahinet et al., 1995) Assume that* $\mathbf{C}$ *is a positive definite matrix. The following relation holds*

$$\mathbf{A} - \mathbf{B}\mathbf{C}^{-1}\mathbf{B}^T \geq 0 \Leftrightarrow \begin{bmatrix} \mathbf{A} & \mathbf{B} \\ \mathbf{B}^T & \mathbf{C} \end{bmatrix} \geq 0. \tag{A.1}$$

■

Appendix B. PHANToM Omni Parameter Identification

The PHANToM parameters are identified without any external payloads using the method proposed in (Taati et al., 2008). In order to identify the PHANToM parameters, the dynamic equation in (15) is linearly parametrized into the following form:

$$\mathbf{Y}(\ddot{\mathbf{q}}, \dot{\mathbf{q}}, \mathbf{q})\boldsymbol{\alpha} = \boldsymbol{\tau}, \tag{B.1}$$

where $\mathbf{Y} \in R^{2\times 8}$ is called the regressor matrix and $\boldsymbol{\alpha} = [\alpha_1, \ldots, \alpha_8]^T \in R^{8\times 1}$ is the vector of robot parameters to be identified. It is seen that

$$\mathbf{Y}^T = \begin{bmatrix} \ddot{q}_1 & 0 \\ \ddot{q}_1 c_{2.3} - 2\dot{q}_1\dot{q}_3 s_{2.3} & 2\dot{q}_1^2 c_3 s_3 \\ \ddot{q}_1 s_{2.3} + 2\dot{q}_1\dot{q}_3 c_{2.3} & -\dot{q}_1^2 c_{2.3} \\ \ddot{q}_1 s_3 + \dot{q}_1\dot{q}_3 c_3 & -\frac{1}{2}\dot{q}_1^2 c_3 \\ \ddot{q}_1 c_3 - \dot{q}_1\dot{q}_3 s_3 & \frac{1}{2}\dot{q}_1^2 s_3 \\ 0 & \ddot{q}_3 \\ 0 & s_3 \\ 0 & c_3 \end{bmatrix}. \tag{B.2}$$

The dynamic model (B.1) is passed through a first order stable low-pass filter of the form $L(s) = \frac{\omega}{\omega+s}$ to avoid acceleration measurements (Taati

et al., 2008). The cut-off frequency of the filter was chosen to be between robot motion frequencies and noise frequencies, namely equal to 8 Hz. It is observed that

$$\mathbf{Y}_L(\dot{\mathbf{q}}, \mathbf{q})\boldsymbol{\alpha} = \boldsymbol{\tau}_L, \tag{B.3}$$

where $\mathbf{Y}_L$ is the filtered regressor matrix and $\boldsymbol{\tau}_L$ is the filtered torque. A sum of 8 sinusoids, 4 sinusoids for each of the joints 1 and 3, with frequencies ranging from 0.2 Hz to 1 Hz were applied to the PHANToM to identify the 8 unknown parameters. Note that the sum of n sinusoids is persistent excitation of an order no less than $2n-2$ (Soderstrom and Stoica, 1989). The first and the third joints of the PHANToM were under PD (proportional-derivative) control and the second joint was locked at 0^{deg}. The recursive least squares algorithm is employed to find the parameters of the PHANToM (Astrom and Wittenmark, 1995).

ACKNOWLEDGEMENT

This work was supported by the Natural Sciences and Engineering Research Council of Canada (NSERC).

References

Armstrong-Hélouvry, B., Dupont, P., Canudas de Wit, C., 1994. A survey of models, analysis tools and compensation methods for the control of machines with friction. Automatica 30, 1083–1138.

Astrom, K.J., Wittenmark, B., 1995. Adatpive Control. Addison Wesley.

Bauchspiess, A., Alfaro, S.C., Dobrzanski, L.A., 2001. Predictive sensor guided robotic manipulators in automated welding cells. J. Mater. Process. Tech. 109, 13–19.

Bickel, R.J., Tomizuka, M., 1995. Disturbance observer based hybrid impedance control, in: Proc. American Control Conference, pp. 729–733.

Bona, B., Indri, M., 2005. Friction compensation in robotics: an overview, in: Proc. IEEE Conf. Decision and Control, pp. 4360–4367.

Cassemiro, E.R., Rosario, J.M., Dumur, D., 2005. Robot axis dynamics control using a virtual robotics environment, in: Proc. IEEE Int. Conf. Emerging Technologies and Factory Automation, pp. 305–311.

Chan, S.P., 1995. A disturbance Observer for robot manipulators with application to electronic components assembly. IEEE Trans. Ind. Electron. 42, 487–493.

Chen, W.H., Ballance, D.J., Gawthrop, P.J., O'Reilly, J., 2000. A nonlinear disturbance observer for robotic manipulators. IEEE Trans. Ind. Electron. 47, 932–938.

Choi, C.H., Kwak, N., 2003. Robust control of robot manipulator by model-based disturbance attenuation. IEEE/ASME Trans. Mechatron. 8, 511–513.

Corradini, M.L., Fossi, V., Giantomassi, A., Ippoliti, G., Longhi, S., Orlando, G., 2012. Discrete time sliding mode control of robotic manipulators: Development and experimental validation. Control Eng. Pract. 20, 816–822.

Cortesao, R., 2007. On Kalman active observers. J. Intell. Robot. Syst. 48, 131–155.

Damaren, C., Sharf, I., 1995. Simulation of flexible-link manipulators with inertial and geometric nonlinearities. Transactions of the ASME 117, 74–87.

Danesh, M., Sheikholeslam, F., Keshmiri, M., 2005. External force disturbance rejection in robotic arms: An adaptive approach. IEICE T. Fund. Electr. E88A, 2504–2513.

Eom, K., Suh, I., Chung, W., Oh, S.R., 1998. Disturbance observer based force control of robot manipulator without force sensor, in: Proc. IEEE Int. Conf. Robot. Autom., pp. 3012–3017.

Eom, K.S., Suh, I.H., Chung, W.K., 1997. Disturbance observer based path tracking control of robot manipulator considering torque saturation, in: Proc. Int. Conf. Advanced Robot., pp. 651–657.

Gahinet, P., Nemirovsky, A., Laub, A. J., C.M., 1995. LMI Control Toolbox: For Use With MATLAB. Natick, MA: The Math Works, Inc.

Hu, R., Muller, P.C., 1996. Independent joint control: estimation and compensation of coupling and friction effects in robot position control. J. Intell. Robot. Syst. 15, 41–51.

Ji, J.K., Sul, S.K., 1995. Kalman filter and LQ based speed controller for torsional vibration suppression in a 2-mass motor drive system. IEEE Trans. Ind. Electron. 42, 564–571.

Katsura, S., Matsumoto, Y., Ohnishi, K., 2003. Modeling of force sensing and validation of disturbance observer for force control, in: Proc. IEEE Conf. Ind. Electron. Society, pp. 291–296.

Katsura, S., Matsumoto, Y., Ohnishi, K., 2010. Shadow robot for teaching motion. Robot. Auton. Syst. 58, 840–846.

Kermani, M.R., Patel, R.V., Moallem, M., 2007. Friction identification and compensation in robotic manipulators. IEEE Trans. Instrum. Meas. 56, 2346–2353.

Khalil, H.K., 1996. Nonlinear Systems. Prentice Hall, 2nd edn.

Khelfi, A.F., Abdessameud, A., 2007. Robust h-infinity trajectory tracking controller for a 6 DOF PUMA 560 robot manipulator, in: Proc. IEEE Int. Conf. Electric Mach. Drives, pp. 88–94.

Kim, B.K., Chung, W.K., 2003. Advanced disturbance observer design for mechanical positioning systems. IEEE Trans. Ind. Electron. 50, 1207–1216.

Kim, Y., Seok, J., Noh, I., Won, S., 2008. An adaptive disturbance observer for a two-link robot manipulator, in: Proc. Int. Conf. Control, Automation and Systems, pp. 141–145.

Komada, S., Machii, N., Hori, T., 2000. Control of redundant manipulators considering order of disturbance observer. IEEE Trans. Ind. Electron. 47, 413–420.

Komada, S., Miyakami, T., Ishida, M., Hori, T., 1996. Simple control strategy of redundant manipulators by disturbance observer, in: Proc. IEEE/IECON Int. Conf. Industrial Electronics, Control, and Instrumentation, pp. 1884–1889.

Lee, C., Chan, S., Mital, D., 1993. A joint torque disturbance observer for robotic assembly, in: Proc. IEEE Circuits Syst., pp. 1439–1442.

Levant, A., 1998. Robust exact differentiation via sliding mode technique. Automatica 34, 379–384.

Liu, C.S., Peng, H., 1997. Disturbance estimation based tracking control for a robotic manipulator, in: Proc. American Control Conference, pp. 92–96.

Liu, C.S., Peng, H., 2000. Disturbance observer based tracking control. ASME Trans. Dyn. Syst. Meas. Control 122, 332–335.

Liu, H., Wei, T., Wang, X., 2009. Signal decomposition and fault diagnosis of a scara robot based only on tip acceleration measurement, in: Proc. IEEE Int. Conf. Mechatron. Autom., pp. 4811–4816.

Marquez, H.J., 2003. Nonlinear Control Systems. Hoboken, NJ: John Wiley & Sons, Inc.

Mohammadi, A., Marquez, H.J., Tavakoli, M., 2011a. Disturbance observer-based trajectory following control of nonlinear robotic manipulators, in: Proc. Canadian Congress of Applied Mechanics, Vancouver, BC. pp. 779–782.

Mohammadi, A., Tavakoli, M., Marquez, H.J., 2011b. Disturbance observer based control of nonlinear haptic teleoperation systems. IET Control Theory Appl. 5, 2063–2074.

Mulero-Martinez, J.I., 2007. Uniform bounds of the Coriolis/centripetal matrix of serial robot manipulators. IEEE Trans. Robot. 23, 1083–1089.

Naerum, E., Cornella, J., Elle, O.J., 2008. Contact force estimation for backdrivable robotic manipulators with coupled friction, in: Proc. IEEE Int. Conf. Intell. Robots Syst., pp. 3021–3027.

Natori, K., Kubo, R., Ohnishi, K., 2007. Transparency of time delayed bilateral teleoperation systems with communication disturbance observer, in: Proc. IEEE Int. Conf. Mechatron., pp. 1–6.

Natori, K., Tsuji, T., Ohnishi, K., 2006. Time delay compensation by communication disturbance observer in bilateral teleoperation systems, in: Proc. IEEE Int. Workshop Adv. Motion Control, pp. 218–223.

Natori, K., Tsuji, T., Ohnishi, K., Hace, A., Jezernik, K., 2010. Time-delay compensation by communication disturbance observer for bilateral teleoperation under time-varying delay. IEEE Trans. Ind. Electron. 57, 1050–1062.

Nikoobin, A., Haghighi, R., 2009. Lyapunov-based nonlinear disturbance observer for serial n-link robot manipulators. J. Intell. Robot. Syst. 55, 135–153.

Ohishi, K., Ohde, H., 1994. Collision and force control for robot manipulator without force sensor, in: Proc. IEEE Int Conf. Ind. Electron., pp. 766–771.

Ohnishi, K., Shibata, M., Murakami, T., 1996. Motion control for advanced mechatronics. IEEE/ASME Trans. Mechatron. 1, 56–67.

Park, S., Lee, S., 2007. Disturbance observer based robust control for industrial robots with flexible joints, in: Proc. Int. Conf. Control, Automation and Systems, pp. 2863–2868.

Parlakci, M., Jafarov, E., Istefanopulos, Y., 2004. New variable structure PD-controllers design for robot manipulators with parameter perturbations. Int. J. Robot. Autom. 19, 134–142.

Pi, Y., Wang, X., 2011. Trajectory tracking control of a 6-dof hydraulic parallel manipulator with uncertain load disturbances. Control Eng. Pract. 19, 185–193.

Rakotondrabe, M., Clevy, C., Rabenorosoa, K., Ncir, K., 2010. Presentation, force estimation and control of an instrumented platform dedicated to automated micromanipulation tasks, in: Proc. IEEE Conf. Automation Science and Engineering, pp. 722–727.

Sato, K., Tsuruta, K., 2006. Adaptive H infinity control method with frictions compensation and disturbance rejection for robotic manipulators, in: Proc. IEEE Int. Conf. Cont. App., pp. 627–632.

Sawut, U., Umeda, N., Park, K., Hanamoto, T., Tsuji, T., 2001. Frictionless control of robot arm with sliding mode observer, in: Proc. Int. Conf. Vehicle Electronics, pp. 61–66.

Shimada, N., Ohishi, K., Kumagai, S., Miyazaki, T., 2010. Smooth touch and force control to unknown environment without force sensor for industrial robot, in: Proc. IEEE Int. Workshop Advanced Motion Control, pp. 36–41.

Sneider, H., Frank, P., 1996. Observer-based supervision and fault detection in robots using nonlinear and fuzzy logic residual evaluation. IEEE Trans. Control Syst. Technol. 4, 274–282.

Soderstrom, T., Stoica, P., 1989. System Identification. Prentice Hall International Ltd.

Spong, M.W., Hutchinson, S., Vidyasagar, M., 2005. Robot Modeling and Control. New York: Wiley.

Taati, B., Tahmasebi, A.M., Hashtrudi-Zaad, K., 2008. Experimental identification and analysis of the dynamics of a phantom premium 1.5a hatpic device. Presence 17, 327–342.

Tan, Y.H., Sun, D., Huang, W.H., Chen, S.H., 2008. Mechanical modeling of biological cells in microinjection. IEEE Trans. Nanobioscience 7, 257–266.

Voglewede, P., Smith, A., Monti, A., 2009. Dynamic performance of a scara robot manipulator with uncertainty using polynomial chaos theory. IEEE Trans. Robot. 25, 206–210.

Zhongyi, C., Fuchun, S., Jing, C., 2008. Disturbance observer-based robust control of free-floating space manipulators. IEEE Syst. J. 2, 114–119.